



Faculty of Electrical Engineering
Department of Control Engineering


Master's thesis

Risk-Aware Planning for Urban Air Mobility

Bc. Jakub Sláma

May 2021

Supervisor: prof. Ing. Jan Faigl, Ph.D.



“Flying is not dangerous; crashing is what is.”

ANONYMOUS AVIATION WISDOM

I. Personal and study details

Student's name: **Sláma Jakub** Personal ID number: **457224**
Faculty / Institute: **Faculty of Electrical Engineering**
Department / Institute: **Department of Control Engineering**
Study program: **Cybernetics and Robotics**
Branch of study: **Cybernetics and Robotics**

II. Master's thesis details

Master's thesis title in English:

Risk Aware Planning for Urban Air Mobility

Master's thesis title in Czech:

Rizikové plánování ve scénářích městské vzdušné mobility

Guidelines:

1. Familiarize yourself with ground risk maps [1], risk assessment in urban air mobility scenarios [2, 3], risk aware path planning [4], curvature-constrained trajectory planning [5], and existing planning approaches to the emergency landing [6].
2. Propose risk map for a selected in-flight aircraft failure model [7].
3. Based on the risk map, develop risk-aware trajectory planning with the option for safe emergency landing guarantee [8].
4. Evaluate performance of the proposed solution and discuss the results regarding realistic scenarios.
5. Possibly deploy the spatial risk aware trajectory planning on a real fixed-wing aerial vehicle.

Bibliography / sources:

- [1] S. Primatesta, A. Rizzo, and A. la Cour-Harbo: Ground Risk Map for Unmanned Aircraft in Urban Environments, *Journal of Intelligent & Robotic Systems*, 97:489–509, 2020.
- [2] X. Hu, B. Pang, F. Dai, and K. H. Low: Risk Assessment Model for UAV Cost-Effective Path Planning in Urban Environments, *IEEE Access*, vol. 8, pp. 150162–150173, 2020.
- [3] D. Truong, and W. Choi: Using machine learning algorithms to predict the risk of small Unmanned Aircraft System violations in the National Airspace System, *Journal of Air Transport Management*, 86:101822, 2020.
- [4] S. Primatesta, G. Guglieri, and A. Rizzo: A Risk-Aware Path Planning Strategy for UAVs in Urban Environments. *Journal of Intelligent & Robotic Systems*, 95:629–643, 2019.
- [5] J. Patrikar, V. Dugar, V. Arcot, and S. Scherer: "Real-time Motion Planning of Curvature Continuous Trajectories for Urban UAV Operations in Wind, International Conference on Unmanned Aircraft Systems (ICUAS), Athens, Greece, 2020, pp. 854–861.
- [6] Pillar Eng: Path planning, guidance and control for a UAV forced landing. Ph.D. dissertation Queensland University of Technology, 2011.
- [7] Aircraft Owners and Pilots Association, 27TH JOSEPH T. NALL REPORT General Aviation Accidents in 2015, 2018.
- [8] P. Váňa, J. Sláma, J. Faigl, and P. Pačes: Any-time trajectory planning for safe emergency landing, *IEEE/RSJ International Conference on Intelligent Robots and Systems (IROS)*. 2018, pp. 5691–5696.

Name and workplace of master's thesis supervisor:

prof. Ing. Jan Faigl, Ph.D., Artificial Intelligence Center, FEE

Name and workplace of second master's thesis supervisor or consultant:

Date of master's thesis assignment: **15.01.2021** Deadline for master's thesis submission: **21.05.2021**

Assignment valid until:

by the end of summer semester 2021/2022

prof. Ing. Jan Faigl, Ph.D.
Supervisor's signature

prof. Ing. Michael Šebek, DrSc.
Head of department's signature

prof. Mgr. Petr Páta, Ph.D.
Dean's signature

III. Assignment receipt

The student acknowledges that the master's thesis is an individual work. The student must produce his thesis without the assistance of others, with the exception of provided consultations. Within the master's thesis, the author must state the names of consultants and include a list of references.

Date of assignment receipt

Student's signature



Declaration

I hereby declare that the presented work was developed independently and that I have listed all sources of the information used within it in accordance with the methodical instructions for observing the ethical principles in the preparation of university theses.

Prague, 21 May 2021

.....
Bc. Jakub Sláma



Acknowledgement

I would like to thank Ing. Petr Váňa for his advice, ideas, and patience during our research cooperation. Many thanks also go to prof. Ing. Jan Faigl, Ph.D., for his shared knowledge and opportunities I got under his supervision. Furthermore, I would like to thank both of them for the experience and knowledge they have taught me. But most of all, I would like to thank my loving family for their endless support and help, without which my studies and this thesis would not be possible.

Abstract

Aircraft in-flight failures cannot be entirely prevented, and they may lead up to a crash of the aircraft. Such a failure poses a risk also to people and properties on the ground, especially in the urban environment. Current state-of-the-art approaches minimize the risk by determining trajectories resulting in less damage in the case of a failure. Thus, they are minimizing the consequences of a failure. However, the risk of an in-flight loss of thrust failure can be eliminated by an emergency landing if a landing site is reachable. Therefore, we propose a novel risk-aware trajectory planning that minimizes risk to people or damage on the ground while an option of safe emergency landing is guaranteed in the loss of thrust. Henceforth, the overall risk is minimized. The proposed method has been empirically evaluated on a simulated realistic urban scenario. A significant risk reduction is achieved compared to the shortest and risk-aware only trajectories, based on the reported results. The proposed risk-aware planning with safe emergency landing seems to be suitable trajectory planning for urban air mobility.

Keywords: safe emergency landing; sampling-based planning; risk-aware planning; urban air mobility

Abstrakt

Porucha letadla během letu může vést až k jeho havárii, což představuje možné riziko i pro osoby a majetek na zemi, a to zejména ve městském prostředí. Vzniku poruchy nelze zcela zabránit, a proto jsou studovány přístupy minimalizující důsledky poruchy, a tedy možná rizika. Jedním z existujících přístupů je plánování trajektorií, které vedou k menším škodám v případě poruchy. Riziko důsledku úplné ztráty tahu během letu může být plně eliminováno bezpečným nouzovým přistáním, pokud je v dosahu místo pro přistání. V této práci proto navrhujeme novou metodu plánování trajektorií, která nejen zohledňuje riziko, ale také garantuje existenci bezpečné trajektorie nouzového přistání v případě selhání motoru. Dopad navrhovaného řešení pro minimalizaci rizika naplánovaných trajektorií byl empiricky vyhodnocen v simulovaném realistickém městském scénáři. V porovnání s nejkratší trajektorií a trajektorií uvažující pouze riziko, plánuje navržená metoda trajektorie s výrazně nižším celkovým rizikem. Proto lze na základě v práci dosažených výsledků konstatovat, že navržené plánování zohledňující riziko s garancí bezpečného nouzového přistání je vhodnou metodou plánování trajektorií pro městskou leteckou mobilitu.

Klíčová slova: bezpečné nouzové přistání; plánování založené na vzorkování; rizikové plánování; městská letecká mobilita



Used Abbreviations

ATAG	Air Transport Action Groupe
ATSB	Australian Transport Safety Bureau
CASA	Civil Aviation Safety Authority
IATA	International Air Transport Association
ICAO	International Civil Aviation Organization
LoT	Loss of Thrust
NASA	National Aeronautics and Space Administration
NTSB	National Transportation Safety Board
PRM	Probabilistic Roadmap
RRT	Rapidly-exploring Random Tree
UAV	Unmanned Aerial Vehicle
VTOL	Vertical Take-Off and Landing

Used Symbols

α	Impact energy in a standardized scenario
β	Impact energy causing a casualty in an unsheltered area
γ	Aircraft impact angle
Γ	Trajectory
Γ_{bal}	Ballistic-fall trajectory
Γ_{LoT}	Emergency landing trajectory
Δ_{step}	Steer constant
Δ_{tol}	Goal tolerance
ξ	Landing configuration
$\hat{\xi}$	Set of all configurations above the landing site ξ
Ξ	Set of landing sites
ρ	Minimum turning radius
θ	Heading angle
ψ	Pitch angle
\mathcal{A}	Aircraft minimum altitude for a safe landing
A	Aircraft model
A_{exp}	Area exposed to a crash
\mathcal{C}	Configuration space
$\mathcal{C}_{\text{free}}$	Obstacle-free part of configuration space
$\tilde{\mathcal{C}}$	Simplified configuration space
\mathbf{D}	Drag force
d	Dimensionality of a configuration space
d_{step}	Maneuver sampling step
\mathbf{E}	Set of edges in a graph
E	Impact energy
\mathcal{G}	Set of possible ballistic falls

G	Gravitational force
G	Graph
\mathcal{H}	Altitude loss function
H	Set of altitudes of interest
h_p	Height of an average person
\mathcal{L}	Trajectory length
k	Number of selected nearest neighbors
\mathcal{M}	Risk of a configuration
M	Ground risk
\mathcal{N}	Normal distribution
\mathcal{O}	Obstacles
\mathcal{P}	Set of impact probability maps
p_{casualty}	Probability of causing a casualty
p_{fail}	Probability of failure
$p_{\text{fail}}^{\text{LoT}}$	Probability of loss of thrust
p_{hit}	Probability of hitting a person
p_{imp}	Impact probability map
Q	Set of possible impact locations
Q_{near}	Set of k nearest neighbors
q	Aircraft configuration, $q \in \mathcal{C}$
q_m	Configuration where the total malfunction occurs
\tilde{q}	Simplified aircraft configuration, $q \in \tilde{\mathcal{C}}$
\mathcal{R}	Risk of a trajectory
r	Radius
r_p	Radius of an average person
r_{uav}	Radius of the aircraft shape circumference
S	Sheltering factor
\mathcal{T}_{alt}	Terrain altitude
t	Time
u	Control input
V	Set of vertices in a graph
v	Aircraft velocity
\mathbf{x}	Aircraft impact location
\mathcal{Z}	No-flight zones map



Contents

1	A Life in the Skies	1
1.1	Popularity of Aviation	2
1.1.1	Popularity of General Aviation	2
1.2	Urban Air Mobility	3
1.3	Failure Consequences	4
1.3.1	Minimization of Crash Probability	5
1.3.2	Minimization of Failure Consequences	5
1.4	A Planner for Least Risky Flight Paths	6
2	Related Work	7
2.1	Generation of a Feasible Trajectory	7
2.2	Emergency Landing in the Case of a Loss of Thrust	9
2.2.1	Landing Site Detection	9
2.2.2	Emergency Landing Determination	10
2.3	Path and Trajectory Planning Algorithms	10
2.3.1	Randomized Sampling-Based Planning Algorithms	11
2.4	Risk Assessment	13
2.5	Risk-Aware Trajectory Planning	13
2.6	Summary	14
3	Problem Statement	15
3.1	Satisfaction of Vehicle Motion Constraints	15
3.2	Trajectory Risk Minimization	16
3.3	Safe Emergency Landing Guarantee	17
3.4	Risk-Aware Trajectory Planning with Safe Emergency Landing Guarantee	18
4	Model of a Ballistic Fall	19
4.1	Ballistic Fall	19
4.2	Impact Probability Map	20

5	Proposed Risk-based RRT* Method with Safe Emergency Landing Guarantee	23
5.1	The Proposed Method	24
5.2	Safe Altitude Map Generation	25
5.3	Maneuver Admissibility Check	27
5.4	Trajectory Risk Assessment	27
6	Influence of Parameters of the Proposed Method	29
6.1	Parameters of Impact Probability Maps	29
6.2	Parameters of Safe Altitude Map	29
6.3	Performance of Risk-based RRT* Algorithm	30
7	Evaluation of the Proposed Risk-aware Trajectory Planning with Safe Emergency Landing Guarantee	33
7.1	Scenario	33
7.2	Specification of the Testing Instances	34
7.3	Reference Methods	36
7.3.1	Shortest Trajectory Planning Reference Method	36
7.3.2	Risk-Aware Trajectory Planning Reference Method	37
7.4	Results	37
7.4.1	Discussion	39
8	Conclusion	41
	Bibliography	43

List of Figures

1.1	Airbus A380	1
1.2	Cessna Skyhawk	3
1.3	An aircraft for urban air mobility as developed by Lilium	4
1.4	Crashed Cessna 172	5
2.1	An example of 2D Dubins maneuvers	8
2.2	An example of parametric curves	9
3.1	An example of ballistic fall and related impact probability	17
3.2	An example of finding a safe emergency landing trajectory	18
4.1	Forces acting on an aircraft during a ballistic fall	19
4.2	An example of ballistic falls based on initial parameters	20
4.3	Generation of impact probability maps	21
5.1	Roadmap expansion of the proposed method	25
6.1	Effects of the number of simulated falls on the impact probability map	30
6.2	A demonstration of the parameters influence on the safe altitude map	31
6.3	Influence of the creation time of the safe altitude map on its quality .	32
6.4	Influence of the goal tolerance to the required planning time	32
7.1	A visualization of the urban scenario map	35
7.2	An example of the found solution	38



List of Tables

7.1	Sheltering factors used in the evaluation of an urban scenario	34
7.2	Trajectory planning instances	34
7.3	Aircraft parameters for the impact probability model	34
7.4	Results	39

List of Algorithms

1	RRT - Rapidly-exploring Random Tree algorithm	11
2	RRT* - Asymptotically optimal Rapidly-exploring Random Tree algorithm	12
3	Creation of the impact probability maps	22
4	Proposed risk-aware RRT*-based algorithm for the least risky trajectory planning	24
5	RRT*-based construction of landing trajectories	26
6	Trajectory admissibility test	27

A Life in the Skies

Humankind has admired birds for their ability to fly, which is why many attempts to fly had been performed during our history. The first successful flight of a human-crewed engine-powered aircraft happened on December 17, 1903. The flight was successfully performed by the Wright brothers near Kill Devil Hills in North Carolina, United States. Although it was a colossal success, the flight lasted only 12 seconds and covered 36.6 meters (Wright et al., 1977). Nevertheless, as we know it today, the era of modern aviation has started on that day.



Figure 1.1: Airbus A380, the largest passenger aircraft in the world, in Etihad Airways livery during a take-off. The aircraft is 73 m long, 24 m high, and it has a wingspan of 80 m. Although the aircraft can carry up to 853 passengers, the typical capacity is 575 passengers. Credits: Airbus¹

The first aircraft had a wooden skeleton covered by fabrics, and it was capable of carrying only the pilot. However, only a century later, modern aircraft are different. In the skies, we can find small aircraft capable of carrying only a few passengers, for example, Cessna 172. Such aircraft measure only a few meters, and they are flying at relatively slow speeds. Those aircraft are commonly referred to as general aviation, and they are usually used for personal

¹<https://airbus-h.assetsadobe2.com/is/image/content/dam/products-and-solutions/commercial-aircraft/a380-family/A380.Etihad.-.In.flight.7.JPG?wid=3626&fit=constrain>

transportation on short distances or hobby flying. We may also find medium aircraft, such as Fokker 100 or ATR-42, that can carry few tens of passengers. Some of those aircraft are powered by propellers, while others already have jet engines. Propeller aircraft can be considered slow compared to jet aircraft already achieving high speeds. Either way, operating such an aircraft is quite expensive, and so they are usually flown between two airports as part of a network of commercial flights. Last but not least, giant aircraft can be found in the sky. Those aircraft can carry up to a few hundred passengers and fly at almost the speed of sound. Their wingspan and length are several tens of meters, and they are built from metals or carbon fibers as they need to be firm but as light as possible to keep their efficiency. An example of the biggest passenger aircraft in the world is depicted in Fig. 1.1.

1.1 Popularity of Aviation

Modern aviation makes long, fast travel possible, as we can go almost anywhere in the world within a single day. Air transportation is very popular because it is an affordable, fast, and convenient way of transportation. Therefore, the aviation industry is an enormous business. According to ICAO (2019), there have been approximately 104 thousand daily flights worldwide in 2019. On those flights, 11.7 million passengers and 159 thousand tons of cargo valued at more than \$18 billion have been transported every day. The aviation industry supported 65.5 million jobs worldwide, including 10.2 million directly created jobs.

Even though air transportation is very popular and makes fast travels around the world possible, it has its limitations. The network of commercial flights consisted of 48 044 routes in 2019, as stated by ATAG (2019). The network has been divided among 1 478 commercial airlines, which has offered significant possibilities for passengers. Although the network and travel options for passengers may seem sufficient, the network of commercial flights served only just under four thousand airports from approximately forty-two thousand airfields around the world. Moreover, commercial flights are based on flight schedules, which is why one may not fly when exactly he or she needs to, especially in the case of flights between smaller airports with fewer flights.

Last but not least, flying on a commercial flight means that one has to get to the airport, through security screenings, and from the airport at the destination. This additional time needed for air travel may take up to few hours, making short-haul flights less attractive and sometimes even longer than taking ground transportation such as train or bus. These are among the reasons why personal air transportation gains popularity, even though it is usually more expensive.

1.1.1 Popularity of General Aviation

General aviation is a term for civil other-than-scheduled air services. The aircraft are usually small, privately owned, and a passenger with a pilot license usually flies the aircraft. This type of transportation has gained popularity. For example, it is very popular in North America, where people often travel long distances. An example of a general aviation aircraft is shown in Fig. 1.2.

The main advantage of general aviation over commercial airlines is flexibility. One can fly whenever it is needed, and the destination is solely on the pilot and passengers. Hence, any airport in the world can be visited if its structure allows a safe landing and take-off. Smaller airfields usually do not have strict security measurements, and since the departure

is on-demand, the extra time needed at the airport prior to departure is almost zero. Thus, general aviation becomes competitive to ground transportation on short distances.

On the other hand, general aviation does not have such strong support as commercial flights. For example, general aviation flights are usually under visual flight rules, which means the pilot decides where to fly and how. On the contrary, commercial flights have to follow orders of air traffic controllers, who control the air traffic in their area to prevent any collisions. Thus, commercial aircraft has strong support if anything goes wrong, but general aviation cannot rely on the help of air traffic controllers.



Figure 1.2: General aviation flights, i.e., non-scheduled civil air flights, are popular, especially in North America, where people often travel long distances. The depicted Cessna Skyhawk, manufactured by Textron Aviation, is among the popular general aviation aircraft. Credits: Textron Aviation²

1.2 Urban Air Mobility

Although general aviation is quite popular nowadays, it is limited mainly to rural areas. The aircraft need a runway for successful landing and take-off, which is not usually possible within cities. The needed infrastructure can be easily built on almost any field. The usage of small aircraft for personal travels on short to medium distances, so-called urban air mobility, is on the rise, and we may expect it will further increase, as stated by Moore (2003). Hence, the urban air mobility market is expected to be huge, and many companies try to bring urban air mobility into cities. A possible aircraft used for urban air mobility is depicted in Fig. 1.3.

However, flying small aircraft within cities poses several challenges, and aircraft intended for urban air mobility are mostly untypical designs. First, there are usually no runways for take-off and landing within cities. Thus, the aircraft must be capable of vertical take-off and landing (VTOL), similar to helicopters. Therefore, aircraft are usually designed as VTOL, but it then transfers into a standard fixed-wing configuration exploiting lift for the flight phase. The second challenge tackles the noise. Standard aircraft are usually noisy, which is not desirable within cities as it would make living uncomfortable. Hence, many designs count on electric propulsion, which is novel in aviation and raises technical challenges.

²https://cessna.txtav.com/-/media/cessna/images/aircraft/piston/skyhawk/exterior-gallery/dbsg-0057_v1.ashx

Last but not least, safety is a big concern. If anything goes wrong and an aircraft crashes within a city center, the damage on the ground may be enormous due to the high population density and properties on the ground. Henceforth, such a situation must be prevented.



Figure 1.3: An electric VTOL aircraft being developed by Lilium. The technology has been successfully verified in-flight in 2019 on a 5-seater aircraft. A 7-seater model intended for production is currently being developed and certified by aviation authorities. The aircraft is expected to enter production in 2024. Credits: Lilium³

1.3 Failure Consequences

Aviation is the safest mean of transportation as it holds the lowest passenger fatalities to traveled passenger miles ratio. Aviation has been about five times safer than railroad transportation, and about 100 times safer than car transportation, in the U.S. between 2000 and 2009 (Savage, 2013). Although aviation is the safest mean of transportation, a failure may still occur at any time. If something goes wrong during the flight, pilots cannot just pull over to solve the problem. The situation needs to be solved during the flight, or the aircraft has to land prior to solving the problem. Therefore, the distressed aircraft gets into a difficult situation, which may lead to a crash.

According to IATA (2021), commercial airlines achieved only 1.38 accidents per million flights. In other words, a person would have to fly daily for 461 years to encounter an accident with at least one fatality. A person would have to fly daily for 20 932 years on average to encounter an accident with 100% fatality. Therefore, it is extremely unlikely to encounter an accident on-board commercial airlines and even less likely to die on-board.

Although general aviation is also very safe, the chances of a crash are higher as the aircraft checks are less extensive, pilots are less trained, and the aircraft usually fly under visual flight rules, i.e., do not receive as much support from air traffic controllers as commercial airliners. Geske (2018) reports that the general aviation accident rate was 4.89 accidents per 10^5 flight hours in the U.S. in 2015. Pilots' mistakes caused about 74 % of those accidents, mechanical issues caused about 16 % of those, and the remaining 10 % were caused by other causes such as bad weather. A crashed general aviation aircraft can be seen in Fig. 1.4.

³https://lilium.com/files/redaktion/refresh_feb2021/newsroom/press_release/lilium_jet_7_seat_render.04.jpg

In the unlikely event of an in-flight failure, aircraft may crash. A crash does not pose a risk only to people on board but also to people and properties on the ground. Because most flights happen over rural areas, the aircraft would likely crash into a field or other uninhabited areas. Thus, the crash would usually cause none or very little damage on the ground. However, the situation is extremely different in the case of flight over urban areas. Population density is very high in those areas, and so is the chance of causing material damage and casualties on the ground.



Figure 1.4: A crashed Cessna 172 near Burra in New South Wales, Australia. The accident was caused by a strong wind gust during landing and ended up without a casualty. Credits: The Transcontinental Port Augusta⁴

1.3.1 Minimization of Crash Probability

The risk due to possible crashes may be defined in various ways ranging from the economic evaluation to the number of casualties (Dalamagkidis et al., 2009; Hu et al., 2020). Regardless of the risk definition, it is wise to minimize the risk induced by the possible crash. Nowadays, the risk of a crash is mitigated mainly by preventing the crash. For example, flying over urban areas in the Czech Republic is limited to altitudes that allow safe emergency landing in the case of an emergency (Civil Aviation Authority, 2019). Thus, the risk of a crash within an urban environment is reduced by reducing the probability of a situation leading to a crash.

Although this approach reduces the possibility of a failure leading to a crash, it does not mitigate the consequences of a crash once it happens. Therefore, the risk may be mitigated by other means as well. First of all, the risk is assessed with regard to a certain failure. The aircraft behavior after a failure can be modeled, and the impact location predicted. Having the impact predictions, one may plan the trajectory to minimize the possible consequences of a failure. Nevertheless, not all failures have to end up by a crash.

1.3.2 Minimization of Failure Consequences

An in-flight failure may lead to a crash. Nevertheless, after some failures, such as loss of thrust (LoT), the aircraft may still be partially controllable. Hence, an emergency landing

⁴<https://www.transcontinental.com.au/story/1880631/crash-land-pilot-lucky-to-walk-away/?cs=1538>

may be possible. A successful emergency landing eliminates the crash, and a risk to people and properties on the ground is minimized.

If the landing site is reachable even with reduced controllability, the aircraft may perform a successful emergency landing (Sláma, 2018). Therefore, a condition of guaranteed reachability of an emergency landing site in the case of a malfunction might be considered during the planning. However, the satisfaction of such a condition usually represents another trajectory planning problem that increases the difficulty of the problem.

1.4 A Planner for Least Risky Flight Paths

The risk of a trajectory shall be minimized to mitigate the consequences of an in-flight failure. One possible approach by Primatesta et al. (2019,2) is based on risk map planning. A risk map quantifying the risk of impacting a particular location is built considering the fall for the given malfunction. Then, the least risky trajectory is found using a risk-aware planner such as Risk-A*. Although the approach minimizes the risk for the predicted falls, it does not consider emergency landings at all. Hence, the aircraft may crash even in the case of partial loss of control that can otherwise perform a safe emergency landing.

On the other hand, approaches by Sláma (2018); Váña et al. (2020b,1) guarantee a safe emergency landing. Thus, if a partial loss of control happens, a safe emergency landing can be performed, and so the induced risk would be zero. However, such an approach does not consider a total failure at all. Hence, the risk induced by such a situation is not mitigated by any means. Therefore, we propose a novel approach to risk-aware trajectory planning for fixed-wing aircraft in urban environments. The approach is based on the risk-RRT* algorithm, and it combines the advantages of both approaches mentioned above. Thus, the final trajectory guarantees a safe emergency landing option in the case of a partial loss of control, such as the herein addressed loss of thrust. Moreover, the risk induced by possible malfunction followed by a ballistic fall is minimized. The proposed approach leads to significantly less risky trajectories than the current state-of-the-art approaches.

Related Work

An in-flight malfunction of an aircraft always poses a risk of a crash. However, a crash in an urban environment could cause severe material damage, injuries, and casualties due to the high concentration of people. Thus, we would like to minimize the risk induced by flying over an urban area. We propose *Risk-Aware Trajectory Planning with Safe Landing Guarantee* problem that combines multiple challenges related to trajectory planning and risk assessment. The challenges include trajectory planning satisfying vehicle motion constraints, landing site determination and emergency landing trajectory planning, risk assessment, and trajectory planning with minimized risk. None of the existing approaches addresses all the challenges (to the best of the authors' knowledge); however, individual challenges have already been addressed separately. Therefore, we present an overview of the most related existing work to the individual challenges.

Approaches to the generation of maneuvers satisfying the motion constraints of the aircraft are described in Section 2.1. Methods for emergency landing planning in the case of loss of thrust are given in Section 2.2. Strategies for path and trajectory planning are summarized in Section 2.3, and multiple risk assessment options for a given trajectory are presented in Section 2.4. Current approaches to risk-aware planning can be found in Section 2.5, and final remarks on the related work are given in Section 2.6.

2.1 Generation of a Feasible Trajectory

A trajectory for an aircraft has to satisfy its motion constraints; it must be feasible. The aircraft motion constraints can be addressed by the Dubins airplane model proposed by Chitsaz and LaValle (2007), which can be utilized as a simplified model of the aircraft for maneuver generation. The model is a three-dimensional extension of Dubins vehicle (Dubins, 1957) modeling the aircraft motion with a constant forward speed as a curvature-constrained path that can be described by

$$\begin{bmatrix} \dot{x} \\ \dot{y} \\ \dot{z} \\ \dot{\theta} \end{bmatrix} = v \begin{bmatrix} \cos \theta \cos \psi \\ \sin \theta \cos \psi \\ \sin \psi \\ u_{\theta} \rho^{-1} \end{bmatrix}, \quad (2.1)$$

where v is a forward velocity, the control input $u_\theta \in [-1, 1]$ controls the change of heading angle θ , ψ stands for a pitch angle, and ρ denotes the aircraft minimum turning radius. Since the changes in heading angle are typically significantly slower than changes in pitch and roll angles, the model allows abrupt changes in pitch and roll angles. McLain et al. (2014) further modified the model to fit the properties of small Unmanned Aerial Vehicles (UAVs).

The goal of trajectory generation is to determine the shortest trajectory that satisfies the motion constraints of the aircraft given by (2.1) and the maximum curvature and pitch angle limitations. For the Dubins vehicle model, the shortest curvature-constrained trajectory in 2D between two points with prescribed heading angles is called Dubins maneuver that consists of straight segments or circular segments with minimum turning radius. An example of maneuvers is given in Fig. 2.1. However, such a closed-form solution does not exist for the three-dimensional space due to pitch angle limitations.

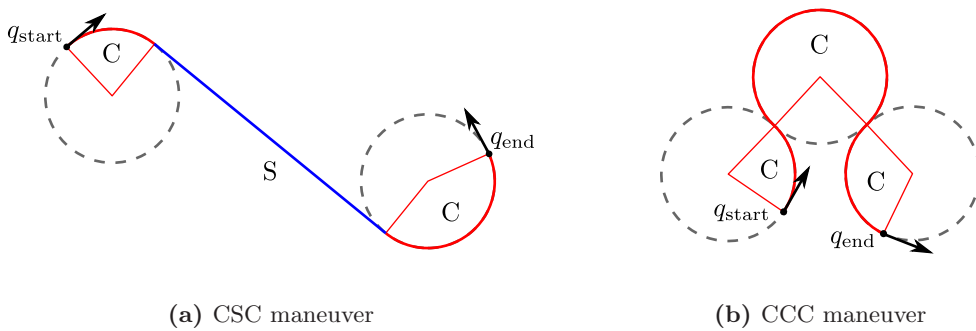


Figure 2.1: An example of 2D Dubins maneuvers.

A generation of length-efficient maneuvers satisfying curvature constraints and pitch limits is studied by Vána et al. (2020a). The authors propose a prolongation of a 3D Dubins maneuver such that the limit pitch angle is achieved if the 3D Dubins maneuver violates the pitch angle limits. A simple 3D Dubins maneuver is constructed by elevating a 2D Dubins maneuver. If the pitch limits are violated, the pitch limit is used for the maneuver, and the altitude difference at the goal location is handled by inserting a spiral segment. The spiral segment would usually gain more altitude than needed if the maximum pitch angle is applied, and the spiral would be unnecessarily long. Thus, Vána et al. (2020a) propose a maneuver with variable turning radii, which can apply the extreme pitch angle during the whole maneuver, resulting in a shorter maneuver.

Wang et al. (2014) propose using a Dubins-Hélix model, a trajectory with spiral (hélix) segments that allows the turning radius projected into the horizontal plane to be smaller than the minimal turning radius. The planned trajectory is shorter than using a 3D Dubins maneuver by Chitsaz and LaValle (2007), but it pushes the aircraft to its limits due to sharp turns during the altitude changes.

The trajectory generation problem can also be addressed by optimization of parametric curves. The used parametrizations in the literature are Bézier curves (Faigl and Vána, 2018; Neto et al., 2015). Bézier curve is a parametric curve defined by two endpoints and at least two other points. However, a Bézier curve cannot be constructed directly with the minimum turning radius; the final trajectory can only be checked to satisfy the curvature constraints. Kan et al. (2011) use trajectory based on B-spline, piecewise polynomial trajectory with multiple segments that consist of Bézier curves. 2D examples of Bézier and B-spline curves are visualized in Fig. 2.2.

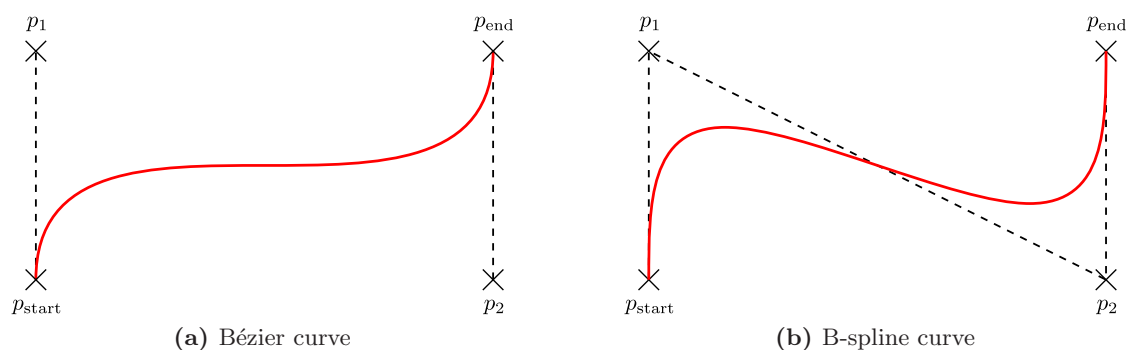


Figure 2.2: An example of parametric curves.

The planned trajectory has to be dynamically feasible for the assumed aircraft, which imposes to be smooth. The trajectory generation can be formulated as a non-linear constrained optimization of the two-point boundary value problem (Patrikar et al., 2020) that can provide collision-free dynamically feasible trajectories in urban areas considering a known wind field in real-time.

Within the context of the herein addressed risk-aware planning, any of the mentioned methods can be utilized depending on the constraints of the utilized vehicle. Because high computational requirements of risk-aware planning are expected, we have decided for the Dubins airplane model (Chitsaz and LaValle, 2007) as it is well-used in the literature and allows fast computations. Besides, it can be substituted by more complex models in the future.

2.2 Emergency Landing in the Case of a Loss of Thrust

An emergency landing can be performed in the case of in-flight loss of thrust, assuming a landing site is within the gliding range of the aircraft. A particular landing site and a corresponding safe emergency landing trajectory need to be selected in such a case.

2.2.1 Landing Site Detection

A method for visually detecting possible landing sites based on RGB images is proposed by Mejias and Fitzgerald (2013). The method relies on edge detection in RGB images, and the edges are expanded to find spare areas. The found areas are then checked in the original image to discard areas unlikely suitable for a landing, and the others are assumed to be possible landing sites.

Another method for visually detecting possible landing sites on rooftops for micro-aerial vehicles is proposed by Desaraju et al. (2015). The proposed method relies on a 3D site reconstruction followed by the detection of locations that provide enough space for an emergency landing and are flat enough.

Humbard and Putman (2007) propose a method of a visual aid for pilots' decision in the case of an emergency landing by visualization of all reachable landing sites to ease the decision. Reachability cones are calculated for all known landing sites, and the reachable landing site is determined. The gliding ratio of the aircraft gives the reachability cone, and it is simply a cone from which the aircraft can glide to the desired location, in this case to the landing site. However, any obstacles nor terrain are not taken into account.

2.2.2 Emergency Landing Determination

Eng (2011) studies emergency landing trajectories in the case of loss of thrust. The method is based on procedures adopted from human-crewed emergency landings stated by CASA (2007). The aim is to have a single-query algorithm providing an emergency landing trajectory that follows several major waypoints around the airport. Although wind is taken into account, obstacles nor terrain are not explicitly considered.

Sláma (2018) proposes RRT*-based algorithm to determine the safest landing site and corresponding gliding trajectory. The author proposes to select a landing trajectory that maximizes the altitude reserve to the terrain. A roadmap is built throughout the whole flight, and in the case of loss of thrust, an emergency landing trajectory is extracted. The method has an any-time feature and based on the reported results; the final trajectory can be extracted almost instantly.

The RRT*-based method has been further extended for the Dubins Traveling Salesman Problem by Váňa et al. (2020b). The proposed method can find the shortest trajectory visiting the given set of locations. At the same time, a safe emergency landing in the case of loss of thrust is guaranteed for any point of the trajectory. Suppose any of the target locations cannot be safely visited because of its insufficient altitude to guarantee emergency landing. In that case, the authors propose a relaxed problem where a feasible and safe solution is found using a safe higher altitude at which the target location is visited than the originally requested unsafe altitude.

According to Atkins (2010), modern airliners already have all key information for a landing site determination: airports and their runways, nearby obstacles, traffic, wind speed, and its direction. The author develops a method for determining the best landing site based on the already possessed information, showing them to pilots, and help them to decide the best landing site available. The proposed method has been evaluated on a real emergency landing data of US Airways Flight 1549, which was forced to ditch into Hudson River in the middle of New York after a loss of thrust shortly after the aircraft take-off.

2.3 Path and Trajectory Planning Algorithms

Path and Trajectory planning is an essential part of the addressed risk-aware trajectory planning problem to determine a cost-efficient path because, for a constant forward velocity, the curvature-constrained path satisfying the vehicle's motion constraints directly represents a trajectory. Therefore, the terms path and trajectory are used as synonyms in this thesis, if not stated otherwise. Two main categories of planning algorithms can be found in the literature. The graph-based search methods such as Dijkstra (Dijkstra, 1959) and A* (Hart et al., 1968) are well-established methods that can be accompanied by incremental search algorithms such as D* Lite (Koenig and Likhachev, 2005) to improve planning performance in the case of the dynamically changing environment. On the other hand, sampling-based methods work directly in continuous configuration space and already demonstrated to be successful approaches, especially for high-dimensional configuration spaces, such as randomized sampling-based approaches such as the Probabilistic Roadmap (PRM) (Kavraki et al., 1996) or Rapidly-exploring Random Tree (RRT) LaValle (1998). Therefore, the representative randomized sampling-based approaches are detailed in the following part of this section.

2.3.1 Randomized Sampling-Based Planning Algorithms

Randomized sampling-based methods sample the continuous space and create its graph representation representing a planning roadmap connecting vertices by a feasible path. In the PRM, the configuration space is randomly sampled into a given number of configurations connected by feasible paths. In practical implementation, not all connections between all sampled configurations are examined, but only k nearest neighbors are selected for each sample to which the sample is being connected (Kavraki et al., 1996). Once the graph (roadmap) is created, a graph-based search method can find the path between two configurations. Thus, the PRM is suitable for multiple queries on the created roadmap.

The RRT algorithm (LaValle, 1998) is a suitable choice for single query planning problems as it incrementally grows a roadmap represented as a tree towards the goal location. The algorithm starts with the initial feasible configuration that forms the root of the tree. Then, the tree is iteratively expanded by choosing a random collision-free sample q_{rand} from the configuration space \mathcal{C} , such that $q_{\text{rand}} \in \mathcal{C}_{\text{free}}$. The `NearestNeighbor` procedure selects the closest configuration q_{near} from the tree, and the control input u moving the vehicle from the random configuration q_{rand} to the nearest configuration q_{near} is determined. A new configuration q_{new} is then created by the `NewConfiguration` procedure and added into the tree. The process is repeated until the termination condition is met, e.g., after a given number of iterations. The algorithm is summarized in Algorithm 1.

Algorithm 1: RRT (LaValle, 1998)

Input: q_{init} – initial configuration
Input: K – number of desired vertices
Input: Δt – time step
Output: G – tree

```

1 Init( $G, q_{\text{init}}$ )
2 for  $k = 1$  to  $K$  do
3    $q_{\text{rand}} \leftarrow \text{RandomConfiguration}()$ 
4    $q_{\text{near}} \leftarrow \text{NearestNeighbor}(q_{\text{rand}}, G)$ 
5    $u \leftarrow \text{SelectInput}(q_{\text{rand}}, q_{\text{near}})$ 
6    $q_{\text{new}} \leftarrow \text{NewConfiguration}(q_{\text{near}}, u, \Delta t)$ 
7   AddVertex( $q_{\text{new}}, G$ )
8   AddEdge( $q_{\text{new}}, q_{\text{near}}, u, G$ )

```

Although the RRT algorithm is probabilistically complete, it might not be asymptotically optimal under certain conditions since the new configuration is connected to the closest configuration in the tree that may not minimize the overall solution cost from the initial to the goal location (Karaman and Frazzoli, 2011). A modified asymptotically optimal variant called RRT* has been proposed by Karaman and Frazzoli (2011). The RRT* grows a tree in a similar randomized manner as the RRT, but the solution improvement is possible by re-connecting nodes in the tree for more cost-efficient trajectories. Using the results on the Randomized Geometric Graphs (Penrose, 2003), the asymptotic optimality can be shown for an increasing number of random samples related to the neighboring function utilized in re-connecting. The RRT* is summarized in Algorithm 2, and it works as follows.

First, a feasible random configuration q_{rand} is sampled, and its closest neighbor q_{nearest} from the tree is found. The found q_{nearest} is extended towards the random sample by applying

Algorithm 2: RRT* (Karaman and Frazzoli, 2011)

```

Input:  $q_{\text{init}}$  – initial configuration
Input:  $\Delta t$  – time step
Output:  $G$  – tree

1 Init( $G, q_{\text{init}}$ )
2 while terminal condition is not met do
3    $q_{\text{rand}} \leftarrow \text{RandomConfiguration}()$ 
4    $q_{\text{nearest}} \leftarrow \text{Nearest}(q_{\text{rand}}, G)$ 
5    $q_{\text{new}} \leftarrow \text{Steer}(q_{\text{nearest}}, q_{\text{rand}})$ 
6   if  $\text{ObstacleFree}(q_{\text{nearest}}, q_{\text{new}})$  then
7      $q_{\text{min}} \leftarrow q_{\text{nearest}}$ 
8      $Q_{\text{near}} \leftarrow \text{Near}(q_{\text{new}}, G)$ 
9     AddVertex( $G, q_{\text{new}}$ )
10    foreach  $q_{\text{near}} \in Q_{\text{near}}$  do
11       $c' \leftarrow \text{Cost}(q_{\text{near}}, q_{\text{new}}) + \text{Cost}(q_{\text{near}})$ 
12      if  $c' < \text{Cost}(q_{\text{min}})$  then
13         $q_{\text{min}} \leftarrow q_{\text{near}}$ 
14    AddEdge( $G, q_{\text{min}}, q_{\text{new}}$ )
15    foreach  $q_{\text{near}} \in Q_{\text{near}} \setminus \{q_{\text{min}}\}$  do
16      if
17         $\text{ObstacleFree}(q_{\text{new}}, q_{\text{near}})$  and  $\text{Cost}(q_{\text{near}}) > \text{Cost}(q_{\text{new}}) + \text{Cost}(q_{\text{new}}, q_{\text{near}})$ 
18        then
19           $q_{\text{parent}} \leftarrow \text{Parent}(q_{\text{near}})$ 
          RemoveEdge( $G, q_{\text{parent}}, q_{\text{near}}$ )
          AddEdge( $G, q_{\text{new}}, q_{\text{near}}$ )

```

a possible action in the **Steer** procedure resulting in the configuration q_{new} closest to q_{rand} . Then, a set of all nodes within the radius r from q_{new} is found by **Near** routine and returned as Q_{near} . The selected radius varies over time and depends on the configuration space dimensionality and the current size of the tree (the number of tree nodes) that is the key factor for the asymptotic optimality of the RRT* (Karaman and Frazzoli, 2011). The new sample q_{new} is connected to a node from Q_{near} that minimizes its cumulative cost from the start location instead of connecting to the nearest one (as in the RRT). Finally, the **Rewire** routine examines all nodes within the set Q_{near} if they can be visited through the newly inserted node at a lower cost.

Determining the nodes within the radius r can be computationally demanding, and therefore k nearest vertices can be used in a practical implementation. However, an arbitrary value of k may lead to non-optimal solutions (Karaman and Frazzoli, 2011), and therefore, k has to satisfy

$$k > 2^{d+1} e \left(1 + \frac{1}{d} \right), \quad (2.2)$$

where d denotes the configuration space dimensionality to assure the asymptotic optimality.

The RRT* algorithm shows to be a powerful planning method with asymptotic optimality of the found solutions, which also satisfies the motion constraints. There are several variants

of the incremental randomized sampling-based methods (Noreen et al., 2016). Kuffner and LaValle (2000) developed the RRT-Connect variant that connects the furthestmost extrapolation of the new sample that improves the performance in particular instances. Besides, the RRT^X by Otte and Frazzoli (2016) is of our particular interest because it is intended for planning with dynamic obstacles using the ideas of the D* Lite algorithm.

2.4 Risk Assessment

An in-flight failure leading to a crash poses a risk of casualties and material loss on the ground if the emergency landing is not possible. In the case of an uncontrolled fall of the aircraft, a precise impact location cannot be predicted. Therefore a stochastic model has to be used, as shown by la Cour-Harbo (2020). The induced risk can be defined in various ways, ranging from the evaluation of economic loss to the number of casualties.

A ground risk map for small UAVs based on the assumed risk to people, ground vehicles and aircraft is proposed by Hu et al. (2020). Since a small UAV has low impact energy and thus does not pose a risk to large objects, a risk to buildings is omitted. However, the assumed simplifications in the approach rely on a uniform distribution of people, ground vehicles, and aircraft on the ground. On the other hand, Dalamagkidis et al. (2009) propose the risk as a probability of three consecutive independent events: (i) loss of control leading to an uncontrolled fall and crash on the ground; (ii) impact with a person on the ground; and (iii) causing a fatality to the hit person.

A ground risk map based on multiple layers is discussed in (Primatesta et al., 2020a) to allow considering various population density and shelter factors given by buildings. The authors propose creating various ground risk maps for various types of failure. However, a fixed flight altitude and only failures leading to total loss of control are assumed. Based on therein reported results, the type of a failure significantly influences its risk map. The final ground risk map is obtained as a linear combination of particular ground risk maps for each failure type weighed by probabilities of failures.

The methods mentioned above predict the impact location or the impact probability based on the aircraft model and its fall. Such a model is sensitive to its parameter settings, which have to be identified with sufficient precision. An alternate approach is to employ machine learning techniques. Truong and Choi (2020) demonstrate the prediction of violation incidents for small UAVs. Although their results show an accuracy of up to 96%, a few thousands of flight data were needed to train the model successfully.

2.5 Risk-Aware Trajectory Planning

Similarly to cost-efficient planning, the least risky trajectory can be obtained by various approaches based on the environment representation. Primatesta et al. (2019) utilize a trajectory risk defined as a sum of risks of flown-over areas and propose using the proposed graph-based variant of the A* algorithm called Risk-A* to find the least risky trajectory in a given roadmap (graph). The main idea is to minimize the cost function

$$f(x) = g(x) + kh(x), \quad (2.3)$$

where $g(x)$ is the motion cost from the start node x_{start} to the end node x , k is the adjustment variable, and $h(x)$ is the heuristic cost that estimates the motion cost between x and the goal

node x_{goal} . The main difference of the Risk-A* compared to the regular A* is that the Risk-A* encapsulates the risk-cost into the function $f(x)$. The motion cost $g(x)$ and heuristic cost $h(x)$ can be expressed for an arbitrary node x_n as

$$g(x) = \int_{x_{\text{start}}}^{x_n} r_c(x) dx, \quad h(x) = \int_{x_n}^{x_{\text{goal}}} r_c(x) dx, \quad (2.4)$$

where function $r_c(x)$ is the risk function. Further assumptions about the risk, such as its limits, are utilized. The Risk-A* approach relies on a multi-layer pre-computed risk map for a static environment limited to a single flight level.

Constructing a whole risk map can be computationally demanding. Therefore, the authors Primatesta et al. (2020b) further explored the idea of a multi-layer ground risk map and proposed an online evaluation of the risk instead of creating a full ground risk map. Hence, an RRT*-based algorithm called risk-based RRT* is proposed for finding the least risky trajectory. The algorithm randomly samples the configuration space, and an impact probability is predicted for the taken sample. Then, the risk is calculated similarly as during the construction of the ground risk map, assuming various map layers such as the population density and sheltering factors. The new sample is added into the roadmap such that the risk is minimized, and the process continues until a trajectory to the goal location is found. The main difference between the risk-based RRT* to RRT* is in incorporating the risk assessment routines. Although the approach allows risk evaluation during the expansion process leading to a significantly reduced computation burden, a fixed flight level is still assumed.

2.6 Summary

The current state-of-the-art in risk-aware trajectory planning consists of approaches by Primatesta et al. (2019,2,2) that allow risk minimization for a fixed flight level. Nevertheless, risk mitigation by guaranteeing a safe emergency landing in the case of a loss of thrust is not considered in these approaches. According to the accident investigations (ATSB, 2016; Geske, 2018), engine failure is more likely to happen than a failure leading to a total loss of control. Hence, elimination of the loss of thrust-induced risk would significantly reduce the overall trajectory risk.

On the other hand, existing methods for trajectory planning with the emergency landing guarantee (Sláma, 2018; Váňa et al., 2020b,1) optimize the trajectory with regards to an emergency landing in the case of loss of thrust. Even though the possibility of a safe emergency landing is guaranteed along the whole trajectory, any other types of failure are not considered in the existing methods.

Based on the literature review, we propose to combine both approaches to minimize the overall risk. The proposed method is based on approaches for emergency landing guarantee to eliminate the risk induced by a possible loss of thrust. Besides, the existing methods for risk-aware trajectory planning are extended to consider various flight levels, and they are used to mitigate the risk induced by other than loss of thrust in-flight failures. Both approaches are combined in the proposed method, while the efficiency for near real-time planning is tackled.

Problem Statement

The goal of the thesis is to provide a solution to the herein studied *Risk-Aware Trajectory Planning with Safe Emergency Landing Guarantee* problem that stands to find a trajectory minimizing the risk of casualties on the ground in the case of an in-flight malfunction. The risk is mitigated by planning the least risky trajectory regarding the loss of controls and guaranteeing a gliding to the nearby landing sites in the case of loss of thrust. The addressed point-to-point trajectory planning problem consists of four identified challenges:

Challenge 1: To satisfy vehicle motion constraints;

Challenge 2: To determine the risk of a trajectory induced by possible in-flight malfunction;

Challenge 3: To find the least risky trajectory; and

Challenge 4: To guarantee a safe emergency landing in the case of loss of thrust.

The individual challenges might be addressed by a specific algorithmic solution; however, the second and the third challenges are tightly related. Thus, they should be addressed simultaneously by the proposed *trajectory risk minimization*.

3.1 Satisfaction of Vehicle Motion Constraints

The planned trajectory has to satisfy the motion constraints of the considered fixed-wing aircraft. Let q be the aircraft configuration. Then, the motion constraints can be described as

$$\dot{q} = f(q), \quad (3.1)$$

where $f(\cdot)$ is a function describing the aircraft model's motion constraints. In our work, the fixed-wing aircraft is modeled as Dubins Airplane (2.1) by Chitsaz and LaValle (2007), repeated here to make the chapter self-contained. The vehicle configuration q consists of its position $(x, y, z) \in \mathbb{R}^3$, a heading angle $\theta \in \mathbb{S}$, and a pitch angle $\psi \in \mathbb{S}$; thus $q = (x, y, z, \theta, \psi)$ and the configuration space is $\mathcal{C} = \mathbb{R}^3 \times \mathbb{S}^2$. The state of an aircraft modeled by Dubins

Airplane can be described as

$$\begin{bmatrix} \dot{x} \\ \dot{y} \\ \dot{z} \\ \dot{\theta} \end{bmatrix} = v \begin{bmatrix} \cos \theta \cos \psi \\ \sin \theta \cos \psi \\ \sin \psi \\ u_\theta \rho^{-1} \end{bmatrix}, \quad (3.2)$$

where v is the forward velocity, the control input $u_\theta \in [-1, 1]$ controls the change of the heading angle θ , and ρ denotes the aircraft minimum turning radius. Dubins Airplane assumes that the pitch angle ψ can be changed significantly faster than the heading angle θ . Therefore, it allows abrupt changes in the pitch angle ψ , given that it is within the aircraft limits, i.e., $\psi \in [\psi_{\min}, \psi_{\max}]$. Since obstacles \mathcal{O} , such as terrain and buildings, are considered, the vehicle motion is limited to be in the collision-free part of the configuration space denoted $\mathcal{C}_{\text{free}}$.

3.2 Trajectory Risk Minimization

A trajectory is required to pose the least possible risk to people on the ground induced by possible in-flight loss of controls over the aircraft. A point-to-point trajectory from $q_i \in \mathcal{C}_{\text{free}}$ to $q_f \in \mathcal{C}_{\text{free}}$ is denoted $\Gamma : [0, T] \rightarrow \mathcal{C}_{\text{free}}$, s.t., $\Gamma(0) = q_i$, $\Gamma(T) = q_f$, and its induced risk \mathcal{R} is given by

$$\mathcal{R} = p_{\text{fail}} \int_0^T \mathcal{M}(\Gamma(t)) dt, \quad (3.3)$$

where p_{fail} is the probability of losing the control and $\mathcal{M} : \mathcal{C}_{\text{free}} \rightarrow \mathbb{R}$ is a function quantifying the risk at a given configuration. If a malfunction happens at the configuration $q_m \in \mathcal{C}_{\text{free}}$, the aircraft falls along a ballistic curve $\Gamma_{\text{bal}} : [0, 1] \rightarrow \mathcal{C}_{\text{free}}$, s.t. $\Gamma_{\text{bal}}(0) = q_m$, until it crashes into the ground (la Cour-Harbo, 2020). The ballistic fall can be described by the motion equation

$$m\dot{\mathbf{v}} = m\mathbf{g} - \frac{1}{2}c\rho S\|\mathbf{v}\|\mathbf{v}, \quad (3.4)$$

where $m\mathbf{g}$ denotes gravity and $\frac{1}{2}c\rho S\|\mathbf{v}\|\mathbf{v}$ denotes Newton's drag force. However, parameters of (3.4), especially of the drag force, are not exactly known as they are saddled with uncertainties. Therefore, the exact fall trajectory with a precise impact location cannot be predicted. Instead, an impact probability map $p_{\text{imp}} : \mathbb{R}^2 \rightarrow \mathbb{R}$ can be determined. An example of such a fall is given in Fig. 3.1.

A risk $\mathcal{M}(q)$ at any configuration q is therefore given as

$$\mathcal{M}(q) = \int_{\mathbb{R}^2} p_{\text{imp}}(\mathbf{x}|\Gamma_{\text{bal}}) M(\mathbf{x}, E, \gamma) d\mathbf{x}, \quad (3.5)$$

where $M(\mathbf{x}, E, \gamma)$ is a ground risk quantifying the possible damage with regards to the impact location \mathbf{x} , the impact energy E , and the impact angle γ . The defined ground risk $M(\mathbf{x}, E, \gamma)$ follows (Primatesta et al., 2020a), where the authors proposed the ground risk at the impact location \mathbf{x} as the probability of casualty given by three consecutive events: (i) aircraft malfunction; (ii) hitting people; and (iii) causing a casualty if a person is hit. In our work, the ground risk consists only of the probability of hitting people p_{hit} , and the probability of causing a casualty if a person is hit p_{casualty} as the probability of failure p_{fail} is incorporated in the trajectory risk (3.3). Therefore, the ground risk can be defined as

$$M(\mathbf{x}, E, \gamma) = p_{\text{hit}}(\mathbf{x}, \gamma) p_{\text{casualty}}(\mathbf{x}, E). \quad (3.6)$$

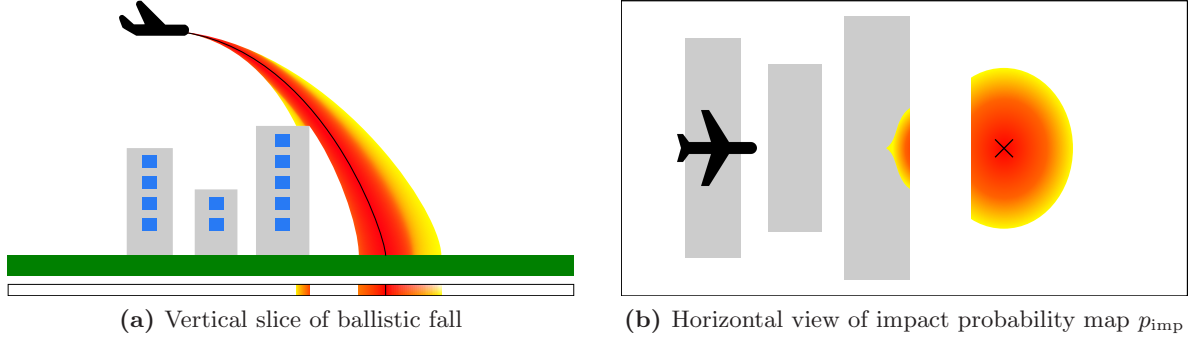


Figure 3.1: An example of ballistic fall and related impact probability with a vertical slice of the situation in (a) and the predicted probability map in (b). The predicted ballistic descent is depicted as a black line surrounded by the probability of aircraft occurrence, where the red shows the highest and yellow the lowest probability. Buildings are represented as gray rectangles. The aircraft falls on top of the rightmost building with a certain probability, but the impact cannot be just next to the building. Most likely, the aircraft falls in the area on the right from buildings with the predicted impact location shown by the black cross.

The probability of hitting a person p_{hit} is adopted from (Primatesta et al., 2020a), and it can be quantified as

$$p_{\text{hit}}(\mathbf{x}, \gamma) = \rho(\mathbf{x})A_{\text{exp}}(\gamma), \quad (3.7)$$

where $\rho(\mathbf{x})$ is the population density at \mathbf{x} , and the area $A_{\text{exp}}(\gamma)$ exposed to the impact is

$$A_{\text{exp}}(\gamma) = 2(r_p + r_{\text{uav}})\frac{h_p}{\tan(\gamma)} + \pi(r_p + r_{\text{uav}})^2 \quad (3.8)$$

with r_p and h_p being the radius and height of an average person, respectively, and r_{uav} being the radius of the aircraft shape circumference.

The probability of casualty is also adopted from (Primatesta et al., 2020a), and it is given as

$$p_{\text{casualty}}(\mathbf{x}, E) = \frac{1 - k}{1 - 2k + \sqrt{\frac{\alpha}{\beta}} \left(\frac{\beta}{E}\right)^{\frac{3}{S(\mathbf{x})}}}, \quad (3.9)$$

where $k = \min\left(1, \left(\frac{\beta}{E}\right)^{\frac{3}{S(\mathbf{x})}}\right)$, $S(\mathbf{x})$ stands to a shelter factor at a location \mathbf{x} , α is the impact energy to achieve $p_{\text{casualty}} = 50\%$ for $S = 6$, and β is the energy needed to cause a casualty in the case of $S \rightarrow 0$. Based on (Standard 321-07, 2007), the value of $\beta = 34 \text{ J}$ is used.

3.3 Safe Emergency Landing Guarantee

The last challenge of the addressed problem is to guarantee a safe emergency landing in the total loss of thrust event. Let $\Xi = [\xi_1, \dots, \xi_m]$ be a set of m possible landing sites with touchdown configurations ξ_i . A trajectory Γ is considered safe in terms of loss of thrust if and only if an emergency landing trajectory $\Gamma_{\text{LoT}} : [0, 1] \rightarrow \mathcal{C}_{\text{free}}$ exists from any point $\tau \in [0, T]$ along the trajectory Γ to the selected landing site $\xi_j \in \Xi$. However, the emergency landing trajectory is not required to end exactly at the selected landing site ξ_j , but at any configuration directly above it as the excess altitude can be quickly lost by specific maneuvers even in the case of

loss of thrust, which has been shown by Váňa et al. (2018). Therefore, $\Gamma(1)$ is from the set $\hat{\xi}_j$ of all configurations directly above ξ_j . The condition of the safe trajectory can be formally written as

$$\forall \tau \in [0, T], \exists \Gamma_{\text{LoT}}, \exists \xi_j \in \Xi : \Gamma_{\text{LoT}}(0) = \Gamma(\tau), \Gamma_{\text{LoT}}(1) = \hat{\xi}_j. \quad (3.10)$$

An example of a safe emergency landing trajectory determination is given in Fig. 3.2.

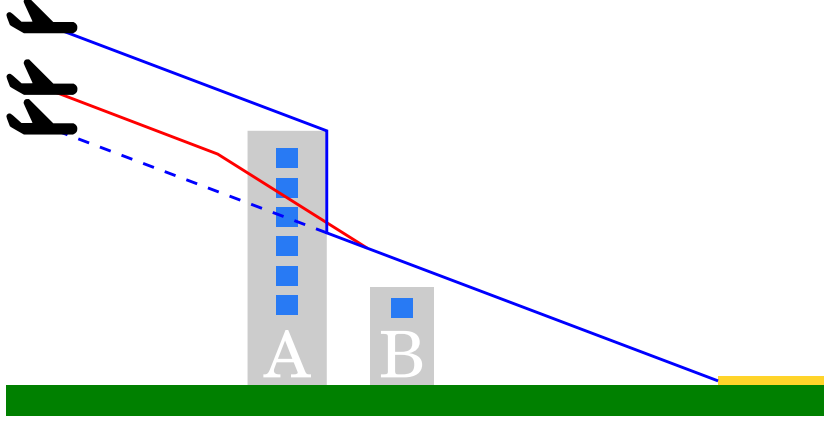


Figure 3.2: An example of finding a safe emergency landing trajectory adopted from (Váňa et al., 2020b). The nearby landing site is on the right, shown as the yellow area. A direct landing trajectory, shown as the dashed blue line, is blocked by buildings, depicted as gray areas. The height of flown-over obstacles determines the minimum safe altitude for a direct flight to the landing site, shown as the solid blue line. The needed altitude for a safe landing can be lowered by flying around obstacles, depicted by the solid red line.

3.4 Risk-Aware Trajectory Planning with Safe Emergency Landing Guarantee

The herein studied point-to-point trajectory planning problem is a combination of the identified challenges. The aim is to determine a feasible trajectory from an arbitrary configuration q_i to an arbitrary final configuration q_f , which minimizes the risk of casualties on the ground in the case of an in-flight malfunction with a guaranteed safe emergency landing if a loss of thrust occurs. The problem can be formally defined as Problem 1, where finding the least risky trajectory is assured by (3.11), and the existence of a safe emergency landing for the whole final trajectory is assured by (3.13). The final trajectory is required to satisfy (3.2) to fulfill the motion constraints of the vehicle.

Problem 1: Risk-Aware Trajectory Planning with Safe Emergency Landing Guarantee

$$\min_{\Gamma} \mathcal{R} = \int_0^T \mathcal{M}(\Gamma(t)) dt \quad (3.11)$$

$$\text{s.t.} \quad \Gamma(0) = q_i, \Gamma(T) = q_f, \quad (3.12)$$

$$\forall \tau \in [0, T], \exists \Gamma_{\text{LoT}}, \exists \xi_j \in \Xi : \Gamma_{\text{LoT}}(0) = \Gamma(\tau), \Gamma_{\text{LoT}}(1) \in \hat{\xi}_j. \quad (3.13)$$

Model of a Ballistic Fall

If a total malfunction occurs, the control over the aircraft is lost, and it falls along a ballistic trajectory until it crashes into the ground. The ballistic fall is described by (3.4). However, its parameters are not exactly known, and so an impact probability map can be obtained rather than a precise impact location. Moreover, the motion equation is a differential equation without an analytical solution requiring a numerical solver to obtain a solution.

4.1 Ballistic Fall

If a total malfunction happens at the configuration q_m , the aircraft starts to fall along a ballistic trajectory $\Gamma_{\text{bal}} : [0, 1] \rightarrow \mathcal{C}$ until it crashes into the ground. Obviously, the fall starts at q_m , and thus $\Gamma_{\text{bal}}(0) = q_m$. The fall is modeled as a ballistic fall, and only gravity and drag forces are assumed, which is visualized in Fig. 4.1. Any other forces are neglected. The gravity is acting in the downwards direction, while the drag force is acting in the opposite direction to the aircraft motion. Hence, the fall can be described by (3.4).

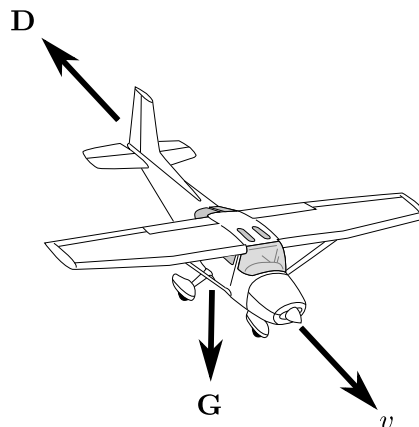


Figure 4.1: Forces acting on an aircraft during a ballistic fall. The gravity \mathbf{G} always acts in the downward direction, and the drag \mathbf{D} acts in the opposite direction to the velocity vector v . All other forces are neglected during a ballistic fall.

An analytical solution of the ballistic fall motion equation is not known, and therefore, the ballistic fall trajectory Γ_{bal} is found by numerical solution. The fall itself is highly influenced by parameters and boundary conditions of the motion equation, which is demonstrated in Fig. 4.2. The parameter values suffer from various sources of uncertainties. For example, an indicated airspeed v may differ from the actual airspeed as the speed measurement is not perfectly precise. Therefore, the fall cannot be precisely predicted, and an impact probability map has to be created instead of predicting a single impact location.

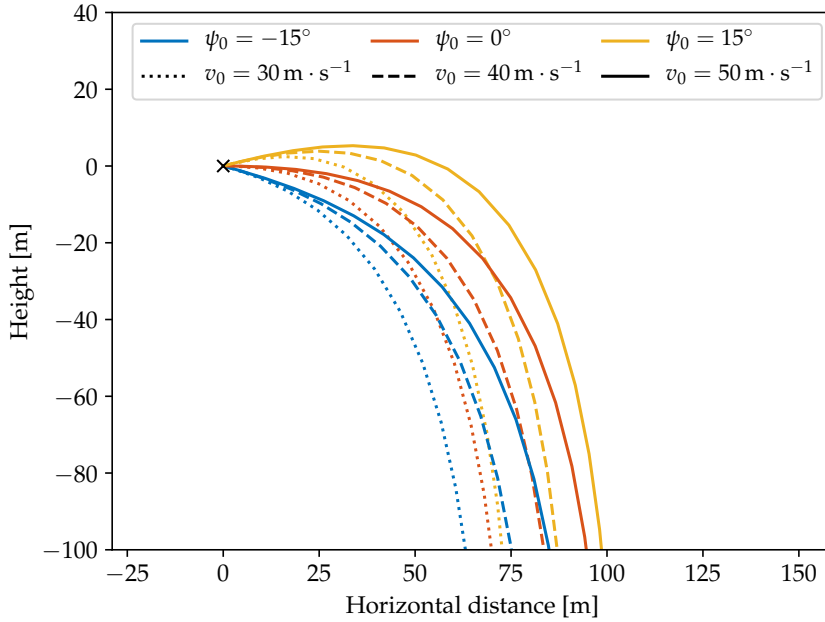


Figure 4.2: An example of ballistic falls based on initial parameters. A total malfunction happens at the configuration denoted by the black cross. A subsequent ballistic fall is shown based on the aircraft speed and pitch angle at the time of the malfunction.

4.2 Impact Probability Map

The impact probability map is determined considering uncertainties in the ballistic fall motion equation parameters and boundary conditions. However, instead of initial altitude and heading, the impact probability map is influenced by a fallen height, i.e., the altitude difference between the initial configuration and the impact location. Besides, if two falls differ only in the initial heading, the falls and impact probability maps are only rotated to each other. Therefore, the impact probability map does not have to be calculated for each malfunction configuration separately but can be pre-computed for individual altitude differences, see Fig. 4.3.

The uncertainties in the parameters of (3.4) are modeled as normal distribution $\mathcal{N}(\mu, \sigma^2)$ with the mean μ and variance σ^2 . The initial velocity v , heading angle θ , pitch angle ψ , and drag coefficient c are assumed to be uncertain, and the other parameters are assumed to be known precisely. Because the analytical solution of the motion equation is not available, the uncertainties of the input parameters and initial conditions cannot be directly transformed into the impact probability map. Therefore, several ballistic falls with known parameters are predicted based on the parameter distributions, and the impact probability map is built

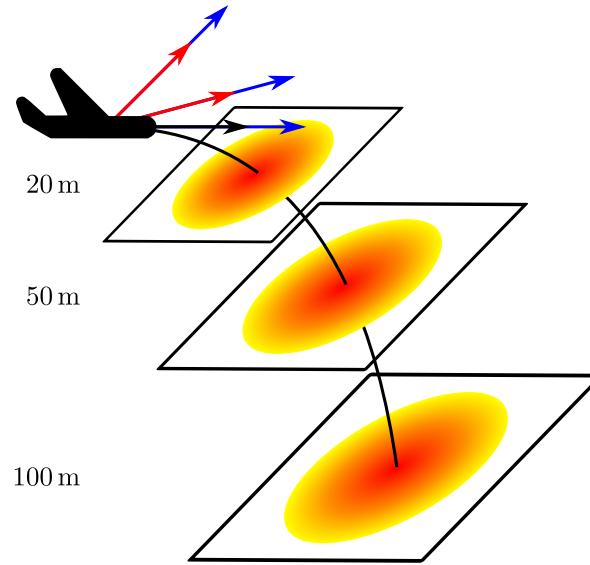


Figure 4.3: An example of impact probability maps generation. A generic ballistic fall (black line) is computed for the initial speed sample (black arrow). Impact probability maps for the selected speed sample are created for the fallen heights of 20 m, 50 m, and 100 m. Similarly, the maps are created for other speed samples (red and blue arrows). If an impact probability map is needed for the fall from the configuration q , the closest map based on the fallen height and initial speed can be taken and aligned to correspond to the position and heading of q .

based on the predicted trajectories. Besides, impact probability maps are constructed for the given fallen heights. The process of generating the impact probability maps is summarized in Algorithm 3, and it goes as follows.

First, random samples of uncertain parameters are created from their distributions for the particular aircraft model A (Lines 4 to 7, Algorithm 3). Then, (3.4) can be solved, e.g., using the `SolveODE` routine (Rackauckas and Nie, 2017), providing a ballistic fall trajectory Γ_{bal} . The found trajectory is added to the set of ballistic trajectories \mathcal{G} , and the process is repeated until n trajectories are determined. Afterward, an impact probability map is created for each fallen height h in the set of altitudes of interest H (Lines 11 to 14, Algorithm 3).

A single impact probability map p_{imp} is created using the aircraft position after falling h meters is determined along all found trajectories \mathcal{G} by the `GetPositions` routine, creating a set of all aircraft positions Q . The aircraft positions are fitted by the normal distribution in the `CreateMap` routine, which provides the impact probability map p_{imp} . Such an impact probability map is created for each fallen height of interest. Thus, a set \mathcal{P} of all impact probability maps is created prior to the next step of risk-based planning with a safe emergency landing guarantee.

Algorithm 3: Creation of the impact probability maps

Input: A – Aircraft model**Input:** H – Set of fallen heights of interest**Parameter:** n – Number of samples**Output:** \mathcal{P} – Set of impact probability maps for fallen heights H

```

1 Function GenerateImpactProbabilityMaps( $A, H$ ):
2    $\mathcal{G} \leftarrow \emptyset$ 
3   for  $i \in 1 : n$  do
4      $c \leftarrow \text{SampleDragCoefficient}(A)$ 
5      $v \leftarrow \text{SampleSpeed}(A)$ 
6      $\theta \leftarrow \text{SampleHeadingAngle}(A)$ 
7      $\psi \leftarrow \text{SamplePitchAngle}(A)$ 
8      $\Gamma_{\text{bal}} \leftarrow \text{SolveODE}(c, v, \theta, \psi)$            // (Rackauckas and Nie, 2017)
9      $\mathcal{G} \leftarrow \mathcal{G} \cup \Gamma_{\text{bal}}$ 
10   $\mathcal{P} \leftarrow \emptyset$ 
11  for  $h \in H$  do
12     $Q \leftarrow \text{GetPositions}(\mathcal{G}, h)$ 
13     $p_{\text{imp}} \leftarrow \text{CreateMap}(Q)$ 
14     $\mathcal{P} \leftarrow \mathcal{P} \cup p_{\text{imp}}$ 
15  return  $\mathcal{P}$ 

```

Proposed Risk-based RRT* Method with Safe Emergency Landing Guarantee

The *Risk-Aware Trajectory Planning with Safe Emergency Landing Guarantee* problem combines multiple challenges that have to be tackled by the proposed solution to solve the problem successfully. Four individual Challenges 1–4 have been identified in Chapter 3 and are repeated here to make this chapter self-contained. The challenges are:

Challenge 1: To satisfy vehicle motion constraints;

Challenge 2: To determine the risk of a trajectory induced by possible in-flight malfunction;

Challenge 3: To find the least risky trajectory; and

Challenge 4: To guarantee a safe emergency landing in the case of loss of thrust.

Although individual challenges have already been addressed in the literature and the individual approaches may be, at least partially, used, the proposed method has to be efficient enough to be computable, which represents one more challenge to make the method usable.

The herein proposed method is based on the risk-based RRT* algorithm (Primatesta et al., 2020b) that is generalized for the use of various flight levels. Furthermore, the trajectory risk is significantly reduced by exploiting safe emergency landing trajectories in the case of loss of thrust adopted from (Vána et al., 2020b). Since the safe emergency landing is guaranteed for the whole trajectory, the risk induced by loss of thrust is eliminated, which is assumed to significantly reduce the overall trajectory risk.¹ The main idea of the proposed method is to grow a risk-aware roadmap until the solution is found. The roadmap is grown backward compared to the original RRT* algorithm (Karaman and Frazzoli, 2011), i.e., from the goal configuration q_f towards the initial configuration q_i . It is because the risk is defined as risk-to-goal, and such a roadmap can be reused if replanning to the same goal location is needed throughout the flight.

¹The hypothesis on the reduction has been empirically validated for the proposed solution, and the supporting results are presented in Chapter 7.

5.1 The Proposed Method

A summary of the proposed generalization of the risk-aware planner (Primatesta et al., 2020b) is depicted in Algorithm 4, and it works as follows. A set \mathcal{P} of the impact probability maps is pre-computed by Algorithm 3. Then, a safe altitude map is created using (Vána et al., 2020b) based on determining the best landing site and corresponding gliding trajectory using the RRT*-based algorithm, detailed in Section 5.2. Once the safe altitude map is created, the planning roadmap G is initialized by the desired destination configuration q_f . Note, the risk-to-goal of the destination configuration is zero.

The planning itself (Lines 5 to 15, Algorithm 4) starts by generating a random sample q_{rand} by the `SampleUniform` routine. The nearest configuration q_{nearest} from the roadmap G is extracted by the `Nearest` routine. If the connection of q_{rand} to the roadmap is longer than the maximum allowed growing step Δ_{step} , the connection is shortened to the maximum

Algorithm 4: Proposed risk-aware RRT*-based algorithm for finding the least risky trajectory and safe emergency landing

Input: A – Aircraft model
Input: H – Set of fallen heights of interest
Input: q_i – Initial configuration of the aircraft
Input: q_f – Final configuration of the aircraft
Input: \mathcal{T}_{alt} – Altitude of the terrain (or obstacles)
Input: \mathcal{Z} – Map of no-flight zones
Output: Γ – The least risky trajectory
Output: $\mathcal{R}(q_i)$ – Risk of trajectory Γ

```

1  $\mathcal{P} \leftarrow \text{GenerateImpactProbabilityMaps}(A, H)$  // call Algorithm 3
2  $G_l, \mathcal{A} \leftarrow \text{SafeLandingMap}(\Xi, \mathcal{T}_{\text{alt}})$  // call Algorithm 5
3  $G \leftarrow \{V \leftarrow q_f, E \leftarrow \emptyset\}$ 
4  $\mathcal{R}(q_f) \leftarrow 0$ 
5 do
6    $q_{\text{rand}} \leftarrow \text{SampleUniform}()$ 
7    $q_{\text{nearest}} \leftarrow \text{Nearest}(q_{\text{rand}}, G)$ 
8    $q_{\text{new}} \leftarrow \text{Steer}(q_{\text{nearest}}, q_{\text{rand}})$ 
9    $Q_{\text{near}} \leftarrow \text{Near}(q_{\text{new}}, G)$ 
10   $q_* \leftarrow \text{argmin}_{q_n \in Q_{\text{near}}} [\mathcal{R}(q_n) + \mathcal{R}(q_{\text{new}}, q_n)]$  // Minimize the risk of new sample
11   $\mathcal{R}(q_{\text{new}}) \leftarrow \mathcal{R}(q_*) + \mathcal{R}(q_{\text{new}}, q_*)$ 
12  if isAdmissible $((q_{\text{new}}, q_*), G_l, \mathcal{A}, \mathcal{T}_{\text{alt}}, \mathcal{Z})$  then
13     $V \leftarrow V \cup \{q_{\text{new}}\}; E \leftarrow E \cup \{(q_*, q_{\text{new}})\}$ 
14     $G \leftarrow \text{Rewire}(Q_{\text{near}}, G)$ 
15 while  $\|q_{\text{new}} - q_i\| < \Delta_{\text{tol}}$ 
16  $Q_{\text{near}} \leftarrow \text{Near}(q_i, G)$ 
17  $q_* \leftarrow \text{argmin}_{q_n \in Q_{\text{near}}} [\mathcal{R}(q_n) + \mathcal{R}(q_i, q_n)]$  // Min. the risk of initial configuration
18  $\mathcal{R}(q_i) \leftarrow \mathcal{R}(q_*) + \mathcal{R}(q_i, q_*)$ 
19 if not isAdmissible $((q_i, q_*), G_l, \mathcal{A}, \mathcal{T}_{\text{alt}}, \mathcal{Z})$  then
20   goto Line 5
21  $\Gamma \leftarrow \text{ExtractTrajectory}(q_i, G)$ 
22 return  $\Gamma, \mathcal{R}(q_i)$ 

```

allowed growing step, and the **Steer** routine creates a new sample q_{new} . Then, a set Q_{near} of k nearest neighbors of q_{new} is determined by the **Near** routine. All possible connections from q_{new} to samples $q_n \in Q_{\text{near}}$ are evaluated to select the best parent q_* leading to the minimal risk $\mathcal{R}(q_{\text{new}})$.

With a slight abuse of notation, let us refer to $\mathcal{R}(q)$ as the total risk from q to q_f while $\mathcal{R}(q_1, q_2)$ refers to the risk of trajectory from q_1 to q_2 . If a maneuver does not guarantee a safe emergency landing in the case of loss of thrust or if it violates any no-flight zone, i.e., it is inadmissible, its risk is considered infinite. The new sample q_{new} is inserted into the roadmap G if the connection to its parent q_* is admissible. The admissibility check is performed by the **isAdmissible** routine that is detailed in Section 5.3. Details of the trajectory risk assessment are provided in Section 5.4. It is worth noting that the rewiring process is needed to assure the asymptotic optimality of the trajectory planning (Karaman and Frazzoli, 2011). Therefore, the **Rewire** routine is called, and samples from Q_{near} are rewired to q_{new} if it reduces risk. An example of a single run of the roadmap expansion is visualized in Fig. 5.1.

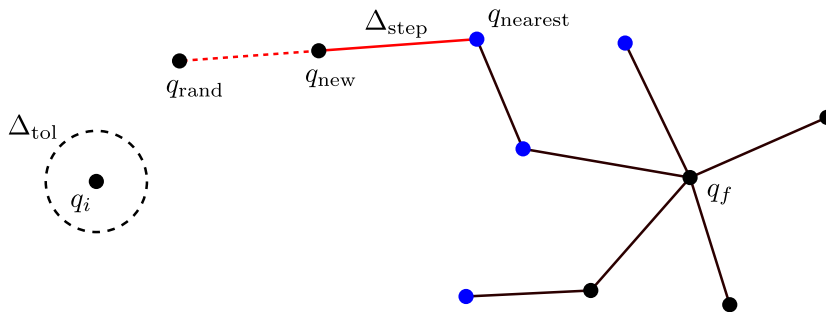


Figure 5.1: An example of a single iteration of the roadmap expansion. The random sample q_{rand} is too far from the nearest node q_{nearest} of the roadmap G . Therefore, a new sample q_{new} is created at the maximum allowed distance Δ_{step} . The best parent is selected from k nearest neighbors (shown in blue) in the roadmap; $k = 4$ is used. The vicinity of the current destination q_i is not reached, and thus the planning continues with the additional iteration.

The roadmap expansion is repeated until the roadmap G reaches the vicinity of the initial configuration q_i within Δ_{tol} . Then, the expansion process is suspended, and the initial configuration q_i is inserted into the roadmap. The insertion process is identical to the insertion of q_{new} ; a set Q_{near} of k nearest neighbors of q_i is extracted from the roadmap by the **Near** routine. All possible connections are evaluated, and the best parent q_* is found. If the connection is admissible, the found trajectory is extracted by the **ExtractTrajectory** routine, and the planning is finished. The roadmap expansion continues with a new random sample otherwise.

5.2 Safe Altitude Map Generation

Determining a safe altitude is a crucial step during the maneuver admissibility check. Finding a minimal safe altitude means that the best landing site and the corresponding gliding trajectory need to be found. Therefore, it is an extensive stand-alone trajectory planning problem. However, the minimum safe altitude is time-invariant, and it is defined solely by the terrain, obstacles, landing sites, and gliding ability of the aircraft. Hence, it can be pre-computed by RRT*-based algorithm adopted from (Vána et al., 2020b) to reduce the computational burden of the risk-aware trajectory planning itself. The algorithm is outlined in Algorithm 5.

The minimum safe altitude is determined for possible emergency landing trajectories based on the gliding aircraft model (Váňa et al., 2018). Therefore, the aircraft configuration is reduced to (x, y) and heading angle θ . The simplified configuration is $\tilde{q} = (x, y, \theta)$ and the simplified configuration space is $\tilde{\mathcal{C}} = SE(2)$, which significantly reduces the computational requirements because of the reduced dimensionality of the planning problem. The altitude of \tilde{q} is assumed to be the minimum altitude allowing a safe emergency landing to some landing site ξ_j from the set of landing sites Ξ . The altitude is denoted as a function $\mathcal{A} : \tilde{\mathcal{C}} \rightarrow \mathbb{R}$. The particular safe altitude is influenced by the selected landing site, terrain altitude \mathcal{T}_{alt} , and the altitude loss $\mathcal{H} : \Gamma_{\text{LoT}} \rightarrow \mathbb{R}$ of the particular landing trajectory Γ_{LoT} .

Algorithm 5: RRT*-based construction of possible emergency landing trajectories
(adopted from (Váňa et al., 2020b))

Input: $\Xi = \{\xi_1, \dots, \xi_m\}$ – Set of the landing sites

Input: \mathcal{T}_{alt} – Altitude of the terrain (or obstacles)

Parameter: t_{plan} – Planning time

Output: G_l – Roadmap of landing trajectories

Output: \mathcal{A} – Minimum safe altitudes for G_l

```

1 Function SafeLandingMap( $\Xi, \mathcal{T}_{\text{alt}}$ ):
2    $G_l \leftarrow \{\mathbf{V} \leftarrow \Xi, \mathbf{E} \leftarrow \emptyset\}$ 
3    $\mathcal{A}(\xi_i) \leftarrow \mathcal{T}_{\text{alt}}(\xi_i), \forall \xi_i \in \Xi$ 
4   while planning time  $t_{\text{plan}}$  has not been reached do
5      $\tilde{q}_{\text{rand}} \leftarrow \text{SampleUniform}()$ 
6      $\tilde{q}_{\text{nearest}} \leftarrow \text{Nearest}(\tilde{q}_{\text{rand}}, G_l)$ 
7      $\tilde{q}_{\text{new}} \leftarrow \text{Steer}(\tilde{q}_{\text{nearest}}, \tilde{q}_{\text{rand}})$ 
8      $Q_{\text{near}} \leftarrow \text{Near}(\tilde{q}_{\text{new}}, G_l)$ 
9      $\tilde{q}_* \leftarrow \text{argmin}_{\tilde{q}_n \in Q_{\text{near}}} [\mathcal{A}(\tilde{q}_n) + \mathcal{H}(\tilde{q}_{\text{new}}, \tilde{q}_n)]$ 
10     $\mathcal{A}(\tilde{q}_{\text{new}}) \leftarrow \max[\mathcal{T}_{\text{alt}}(\tilde{q}_*, \tilde{q}_{\text{new}}), \mathcal{A}(\tilde{q}_*) + \mathcal{H}(\tilde{q}_{\text{new}}, \tilde{q}_*)]$ 
11     $\mathbf{V} \leftarrow \mathbf{V} \cup \{\tilde{q}_{\text{new}}\}; \mathbf{E} \leftarrow \mathbf{E} \cup \{(\tilde{q}_*, \tilde{q}_{\text{new}})\}$ 
12     $G_l \leftarrow \text{Rewire}(Q_{\text{near}}, G)$ 
13  return  $G_l, \mathcal{A}$ 
    
```

The algorithm is very similar to Algorithm 4, as it is also based on the RRT* algorithm. The creation of a safe altitude map starts with the insertion of all landing sites $\xi \in \Xi$ into the roadmap G_l . Then, a random sample \tilde{q}_{rand} is created, and its nearest neighbor from G_l is found by the **Nearest** routine. If the connection is too long, it is shortened, and a new sample \tilde{q}_{new} is created by the **Steer** routine. The set Q_{near} of k nearest neighbors to \tilde{q}_{new} is created by the **Near** routine. All possible connections are evaluated, and the best parent \tilde{q}_* leading to the minimum safe altitude $\mathcal{A}(\tilde{q}_{\text{new}})$ is selected. The minimum safe altitude $\mathcal{A}(\tilde{q}_{\text{new}})$ is determined as a sum of the altitude of the parent and the altitude loss \mathcal{H} of the maneuver from \tilde{q}_{new} to \tilde{q}_* . However, such a maneuver can collide with the terrain. If so, it is discarded as infeasible, and the colliding maneuver is elevated until it is collision-free since every maneuver is assumed feasible if it is high enough. Therefore, the altitude of $\mathcal{A}(\tilde{q}_{\text{new}})$ can also be given as the minimum altitude allowing a safe gliding to its parent configuration in the tree. The safe altitude $\mathcal{A}(\tilde{q}_{\text{new}})$ is given as the maximum of the two aforementioned cases (Line 10, Algorithm 5).

Once the minimum safe altitude at \tilde{q}_{new} is determined, the sample is inserted into the

roadmap G_l . The `Rewire` routine is called to examine connecting samples from Q_{near} through the new sample to assure the asymptotic optimality (Karaman and Frazzoli, 2011). The creation of a safe altitude map continues until the dedicated time t_{plan} elapses.

5.3 Maneuver Admissibility Check

During the proposed risk-aware trajectory planning, maneuvers are examined to be admissible using the minimum safe altitude map \mathcal{A} and validation with respect to the no-flight zones maps \mathcal{Z} . Thus, a maneuver is admissible if it does not violate the minimum safe altitude and no-flight zones. The test itself is carried out by the `isAdmissible` routine summarized in Algorithm 6.

Algorithm 6: Trajectory admissibility test

Input: Γ – Trajectory to be tested
Input: G_l – Roadmap of landing trajectories
Input: \mathcal{A} – Minimum safe altitudes for graph nodes
Input: \mathcal{T}_{alt} – Altitude of the terrain (or obstacles)
Input: \mathcal{Z} – Map of no-flight zones
Output: Admissibility of trajectory Γ

```

1 Function isAdmissible( $\Gamma, G_l, \mathcal{A}, \mathcal{T}_{\text{alt}}, \mathcal{Z}$ ):
2   forall  $q \in \text{SamplePath}(\Gamma)$  do
3      $\tilde{q} \leftarrow \text{Projection2D}(q)$ 
4      $Q_{\text{near}} \leftarrow \text{Near}(\tilde{q}, G_l)$ 
5      $\tilde{q}_* \leftarrow \text{argmin}_{\tilde{q}_i \in Q_{\text{near}}} [\mathcal{A}(\tilde{q}_i) + \mathcal{H}(\tilde{q}, \tilde{q}_i)]$ 
6      $\mathcal{A}(\tilde{q}) \leftarrow \max[\mathcal{T}_{\text{alt}}(\tilde{q}_*, \tilde{q}), \mathcal{A}(\tilde{q}_*) + \mathcal{H}(\tilde{q}_{\text{act}}, \tilde{q}_*)]$ 
7     if  $q \in \mathcal{Z}$  or  $\text{Altitude}(q) < \mathcal{A}(\tilde{q})$  then
8       return false
9   return true

```

First, the maneuver is uniformly sampled with a sampling step d_{step} by the `SamplePath` routine, and the minimum safe altitude is determined for each sample. A 2D projection \tilde{q} is created for each sample q . Similarly, as in Algorithm 5, a set Q_{near} of k nearest neighbors to \tilde{q} is created, and all possible connections are evaluated. The best parent leading to minimum altitude $\mathcal{A}(\tilde{q})$ is determined (Lines 4 to 6, Algorithm 6). The maneuver is assumed as admissible if all samples q are above the minimum safe altitude $\mathcal{A}(\tilde{q})$ and do not violate any no-flight zone \mathcal{Z} .

5.4 Trajectory Risk Assessment

A key feature of risk-aware trajectory planning is the ability to determine the risk Γ of trajectory between two configurations. A risk of a trajectory Γ is determined by (3.3), while the risk of configuration q is given by (3.5). However, both risks are defined continuously and involve integration that would be too computationally demanding. Therefore, a discrete computation is used in the developed implementation of the proposed method. Besides, the risk itself is highly dependent on the impact probability and world properties such as terrain

altitude and population density. Uncertainties define the impact probability in the ballistic fall described by (3.4).

On the other hand, the impact probability depends on the fall height and initial vehicle speed rather than on the actual initial configuration. Hence, the pre-computed impact probability maps are utilized that further reduces the computation burden of the risk assessment. The calculation of the trajectory risk is performed as follows.

Let assumes the trajectory Γ is uniformly sampled with a step d_{step} , and thus a set of n samples $[q_1, q_2, \dots, q_n]$ is created. Then, the trajectory risk (3.3) can be rewritten as

$$\mathcal{R} = p_{\text{fail}} \sum_{i=1}^{n-1} \mathcal{M}(q_i) \frac{\mathcal{L}(q_i, q_{i+1})}{v}, \quad (5.1)$$

where $\mathcal{L}(q_i, q_{i+1})$ denotes the length of the i -th trajectory segment, and v is the aircraft speed. Similarly, we can consider discretized world model, and the configuration risk is computed as

$$\mathcal{M}(q) = \sum_{\mathbb{R}^2} p_{\text{imp}}(\mathbf{x} | \Gamma_{\text{bal}}) M(\mathbf{x}, E, \gamma), \quad (5.2)$$

where p_{imp} is a 2D impact probability map.

The possible impact probability maps can be pre-computed and then used in multi-query risk-aware trajectory planning without further computational requirements. If an impact probability map is needed for a ballistic fall from q , the fallen height is determined based on q and the surrounding terrain. Then, the most appropriate impact probability map p_{imp} can be selected from the available pre-computed impact probability maps \mathcal{P} , and properly aligned to match the position and heading of the vehicle at q , leading to an impact probability map for a ballistic fall starting at the given configuration.

Influence of Parameters of the Proposed Method

The proposed method consists of several parts, and each part's parameters influence the overall performance. Therefore, proper parametrization is essential to achieve the best results. Based on the preliminary evaluation of the proposed method, we identified three main parts that need to tune the parameters: (i) creation of impact probability maps; (ii) the safe altitude map; and (iii) the risk-aware planning itself. The most influencing parameters and their effects are discussed in this chapter.

6.1 Parameters of Impact Probability Maps

Due to uncertainties in parameters estimation of the motion model (3.4), we evaluate the effect of the parameters using randomly sampled values and multiple possible ballistic falls. Possible impact locations are identified based on the found trajectories, and the impact probability map is constructed. We found it important to properly select the number of used ballistic trajectories to compute the map. Therefore, we examine the influence of the number of samples for the uncertain parameters.

The impact probability map is a normal distribution based on the possible impact locations. Therefore, an insufficient number of samples may lead to unrealistic distribution. On the other hand, the motion equation needs to be solved numerically. Thus, finding a single trajectory is relatively computationally expensive. If the number of samples is too high, it can be very demanding but negligible on the map accuracy. We examined impact probability maps computed using several simulated falls up to 25 000 and 2 500 falls seem to be a suitable trade-off between the computational requirements and the resulting impact probability distribution. Three examples of the map distributions are shown in Fig. 6.1.

6.2 Parameters of Safe Altitude Map

The safe altitude map is created by RRT*-based algorithm (Váňa et al., 2020b) that is an extended version of the safe emergency landing algorithm Váňa et al. (2018). As the algorithm is based on the RRT*, it is influenced by the maximal growing step Δ_{step} and the number of the

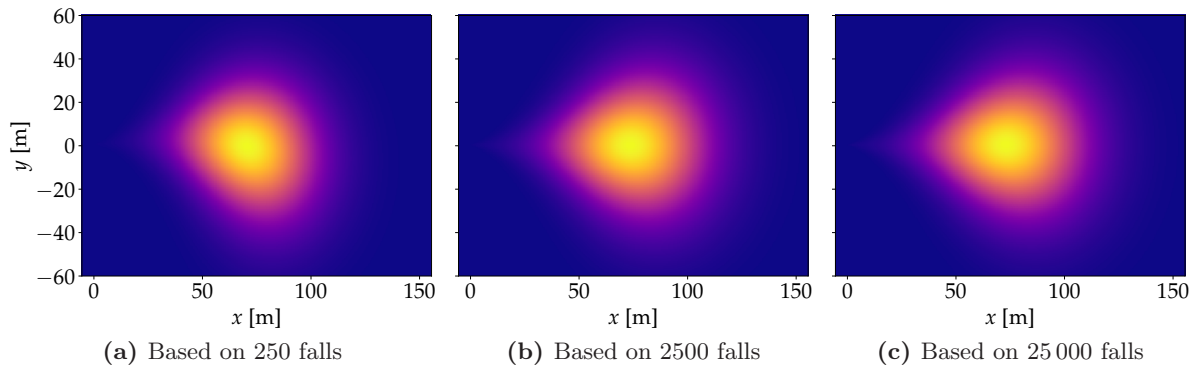


Figure 6.1: Examples of the impact probability map based on the number of simulated ballistic falls. The simulated malfunction happened at $[0, 0]$ with the aircraft flying directly to the right. If too few simulated falls are used for the impact probability map construction, the map might be inaccurate, as shown in (a), where the map is too deviated in the $-y$ direction. It can be noticed in (b) and (c) that increasing the number of falls does not further improve the resulting impact probability map. Hence, 2500 falls have been selected as a suitable number of samples.

nearest neighbors k to which a new sample is tried to be connected to. The influence of those parameters is discussed in detail in (Sláma, 2018). Generally, a higher k yields better solutions at the cost of the increased computational burden. A longer Δ_{step} leads to a faster exploration of the configuration space, but the roadmap is winding. Therefore, both parameters influence the density of the nodes in the final roadmap, as indicated in Fig. 6.2. Besides, the number k of nearest neighbors has to satisfy (2.2) to assure the asymptotic optimality of the algorithm. Since the configuration space has a dimensionality of $d = 3$, the algorithm is asymptotically optimal for any $k \geq 58$.

Furthermore, the safe altitude map creation is also influenced by the planning time t_{plan} for which the roadmap is being expanded. The longer the planning time is, the higher node density in the roadmap is achieved. A denser roadmap may reduce the required altitude at the query location as it is derived from the closest node of the roadmap. On the other hand, increasing the node density in the roadmap beyond a certain value will no longer improve the roadmap as the minimum safe altitude at the query point would stay almost the same. The influence of the roadmap density on the required altitude allowing a safe emergency landing is shown in Fig. 6.3.

Therefore, a suitable trade-off in the parameters settings allows a fast roadmap construction with sufficient quality. The selected values are $k = 60$ and $\Delta_{\text{step}} = 300$ m; however, the planning time t_{plan} needs to be selected according to the size of the planning area to achieve the desired density. We found out that a roadmap density of about 200 nodes/km² seems to provide reasonable results, as indicated in Fig. 6.3. Thus, instead of planning time, we can expand the safe altitude map until the density is reached.

6.3 Performance of Risk-based RRT* Algorithm

The same parameters influence the performance of the proposed risk-based RRT* algorithm itself as of any RRT* algorithm, i.e., the maximum growing step Δ_{step} and the number k of nearest neighbors for testing new sample connection with the roadmap. The parameters influence is identical to the case of the safe altitude map; hence, increasing k improves the solution but for increased computational burden, and increasing Δ_{step} speeds up the spatial

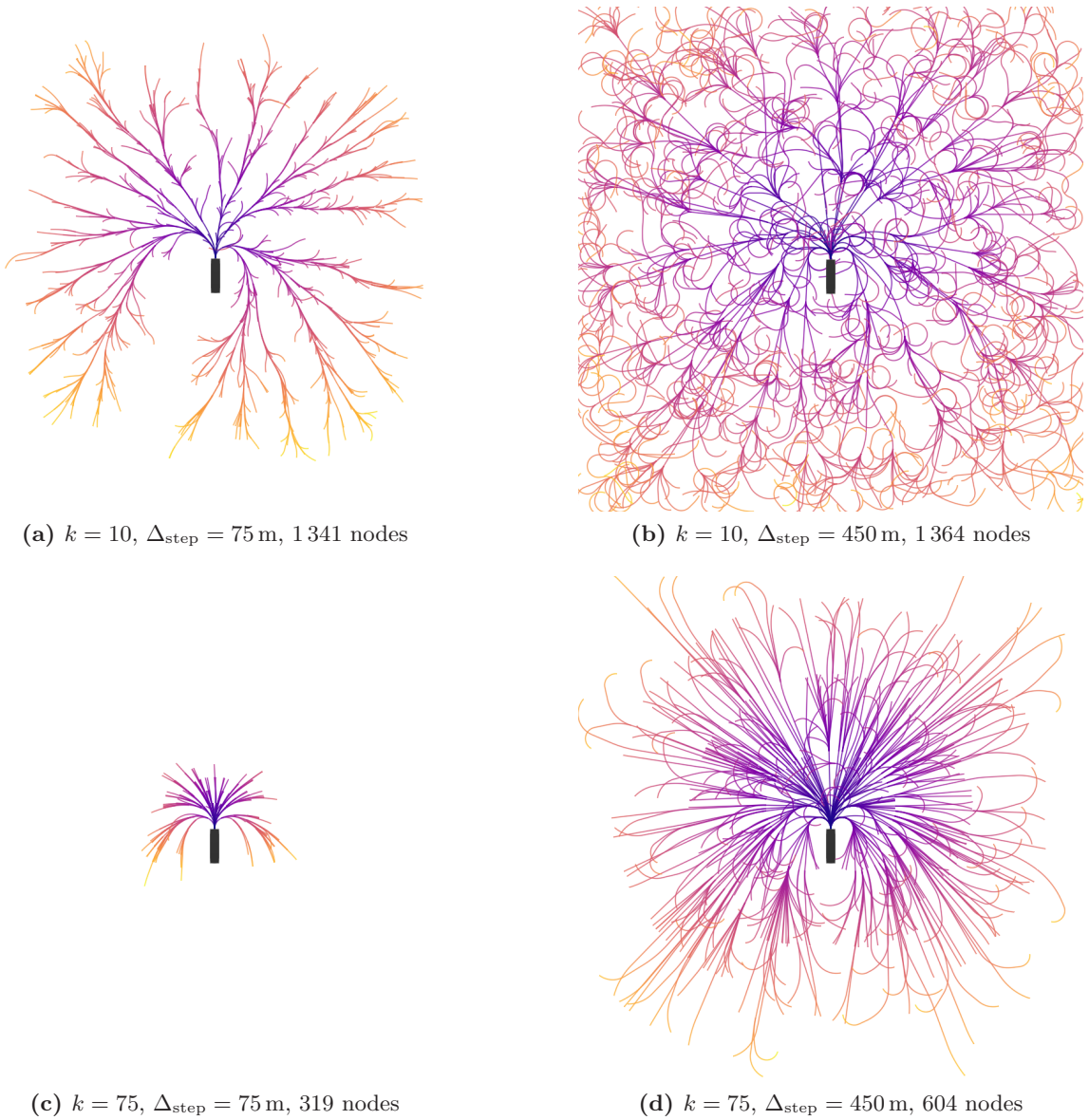


Figure 6.2: Examples of safe altitude maps grown for 60s in a rectangular area 3km large with various parameter settings. The number of examined nearest neighbors k and the maximum allowed growing step Δ_{step} significantly influence the resulting safe altitude map in terms of covered area, number of inserted nodes, and the roadmap branching.

exploration but makes the solution more winding. According to (2.2), k must satisfy $k \geq 109$ to ensure the asymptotic optimality as the dimension of the configuration space is $d = 4$.

Furthermore, the performance is also influenced by Δ_{tol} , which determines the distance from the initial configuration q_i that needs to be reached by the roadmap to terminate the planning. Hence, the longer the distance is, the faster planning ends. However, the initial configuration is then inserted into the roadmap by a single maneuver, and for a long distance, it may not avoid high-risk areas. The influence of the value Δ_{tol} on the needed planning time is depicted in Fig. 6.4.

The relatively high values of k for the asymptotic optimality are prohibitively computa-

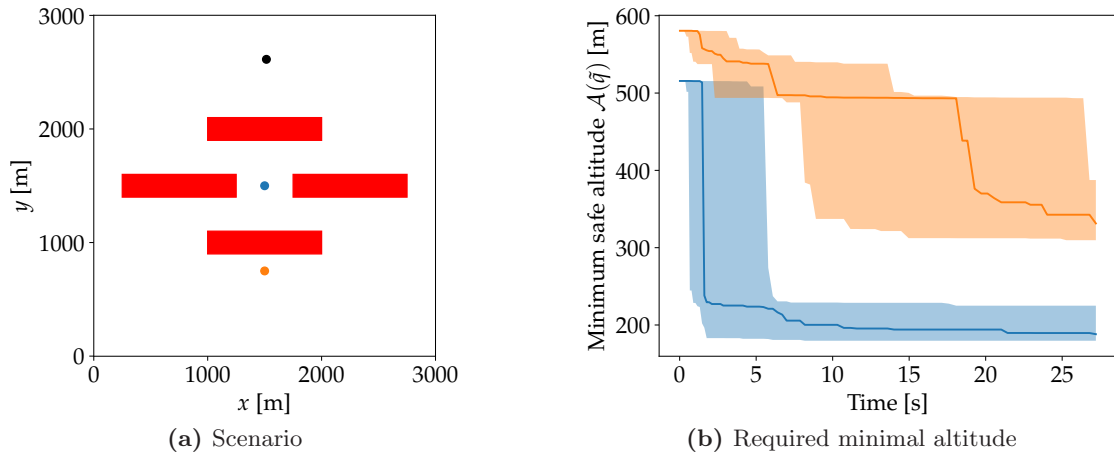


Figure 6.3: Influence of the creation time of the safe altitude map on the map quality in the scenario with a single landing point (black disk), two query points (color disks), and 450 m tall obstacles (red rectangles). The scenario is visualized on the left and the minimum safe altitude at the query points over the safe altitude map construction time is on the right. In the beginning, the landing trajectories lead over obstacles. As the roadmap expands, the minimum safe altitude is decreasing. Growing the roadmap further does not improve the minimum safe altitude after a certain roadmap density. The median and 90% non-parametric confidence interval from 20 trials are shown.

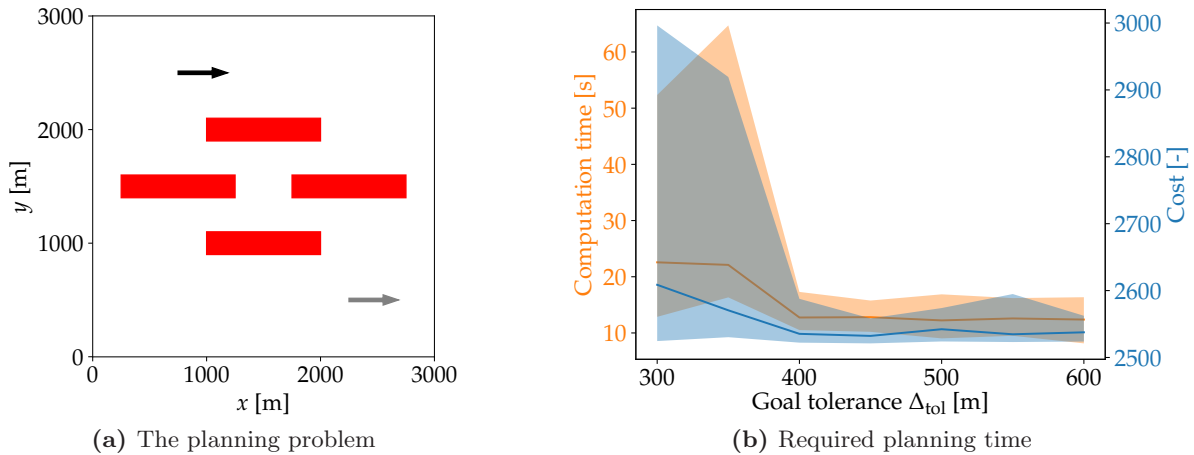


Figure 6.4: An example of effects of the goal tolerance Δ_{tol} on the algorithm performance. The scenario features several obstacles (red rectangles) with a height of 450 m. The task is to find the least risky trajectory from the initial configuration (black arrow) to the final configuration (gray arrow). The scenario is depicted in (a), and results are depicted in (b). Median and 90% non-parametric confident intervals from 20 runs are shown.

tionally demanding to use the algorithm in near real-time deployments because of too many maneuvers to be computed. Therefore, we propose to relax the asymptotic optimality and use $k = 20$ and $\Delta_{\text{step}} = 450$ m for near real-time computations. However, for the offline planning with the asymptotic optimality guarantee, we suggest $k = 110$ for a high-quality solution. Nevertheless, these two settings are empirically evaluated with $\Delta_{\text{tol}} = \Delta_{\text{step}} = 450$ m that minimizes the required planning time while the solution quality is maintained as the length of the initial configuration connection is not longer than the maximum growing step Δ_{step} .

Evaluation of the Proposed Risk-aware Trajectory Planning with Safe Emergency Landing Guarantee

A novel risk-aware trajectory planning method is proposed in this thesis. The method is based on eliminating the risk induced by possible in-flight loss of thrust by guaranteeing safe emergency landing and minimizing the risk of the total in-flight failure by planning the least risky trajectory. The proposed method is evaluated on a realistic urban scenario to demonstrate its behavior and practical performance. The solution found by the proposed method is compared with the shortest trajectory found using the RRT* algorithm without considering risk and safe emergency landing guarantee. Besides, the solutions are compared with the least risky trajectory without the guaranteed emergency landing found by the risk-aware RRT* algorithm (Primatesta et al., 2020b) that has been generalized to various flight levels.

In the rest of this chapter, the evaluation scenario is introduced, followed by the detailed specification of the problem instances used in the empirical evaluation presented in Section 7.2. The reference methods are briefly described in Section 7.3, and the empirical results are reported in Section 7.4.

7.1 Scenario

Today's cities are not prepared for personal air mobility, with daily routes providing a typical scenario for trajectory planning. Therefore, an artificial urban scenario has been prepared for the empirical evaluation of the proposed method. Nevertheless, real data have been used to make the scenario as realistic as possible. The scenario is based on the Prague city center obtained from (OpenStreetMap, 2021), and it is $5 \text{ km} \times 5 \text{ km}$ large. The terrain profile has been obtained from (NASA, 2013) combined with the obstacle heights given in the map. The used population density is based on data (Facebook, 2016), with approximately $1.1 \cdot 10^5$ people living in the scenario area. All town squares within the assumed scenario area have been denoted as no-flight zones to simulate a ban of flights above crowds. Besides, possible

sheltering factors are adopted from (Primatesta et al., 2020a), and the utilized values are summarized in Table 7.1.

Table 7.1: Sheltering factors of particular area types.

Sheltering Factor [-]	Area Type
2.5	Sparse tree, overhead wires, etc.
5.0	Low buildings, forests
7.5	High buildings

There are not any real possible landing sites within the city center. Hence, three landing sites with bi-directional runways have been placed around the scenario map. The simulated landing sites have been placed on the outskirts of the city center in realistic locations such as wide-open areas. The created scenario is visualized together with all map layers in Fig. 7.1.

7.2 Specification of the Testing Instances

Multiple instances of randomly placed initial and final configurations are created on top of the created Prague urban scenario. The initial and final configurations, q_i and q_f , respectively, are randomly placed within the scenario boundary at an altitude of [300 m, 800 m] and with a random heading angle $\psi \in [0, 2\pi)$. The created trajectory planning instances are documented in Table 7.2.

Table 7.2: Trajectory planning instances.

Configurations	
q_i [°N, °E, m, °]	q_f [°N, °E, m, °]
(50.10, 14.40, 482, 222)	(50.08, 14.39, 792, 226)
(50.08, 14.42, 531, 331)	(50.11, 14.43, 550, 79)
(50.08, 14.43, 450, 0)	(50.11, 14.42, 750, 180)
(50.09, 14.42, 742, 316)	(50.12, 14.40, 596, 36)
(50.08, 14.40, 350, 0)	(50.12, 14.45, 350, 0)

Cessna 172, as one of the most popular general aviation aircraft, is selected for aircraft model in the empirical evaluation of the proposed planning method. The model is adopted from (Vána et al., 2018), where the aircraft gliding abilities are described. The model has been further extended by the ballistic fall option. The impact probability model is built based on various ballistic fall predictions described in Chapter 4. The uncertainties used for the predictions are summarized in Table 7.3.

Table 7.3: Aircraft parameters used for the impact probability model. Note that a normal distribution with the mean μ and variance σ^2 is denoted as $\mathcal{N}(\mu, \sigma^2)$.

Parameter	Symbol	Value
Speed	v	$\mathcal{N}(33.4, 10) \text{ m s}^{-1}$
Heading	θ	$\mathcal{N}(0, 15)^\circ$
Pitch angle	ψ	$\mathcal{N}(0, 15)^\circ$

Chapter 7. Evaluation of the Proposed Risk-aware Trajectory Planning with Safe Emergency Landing Guarantee

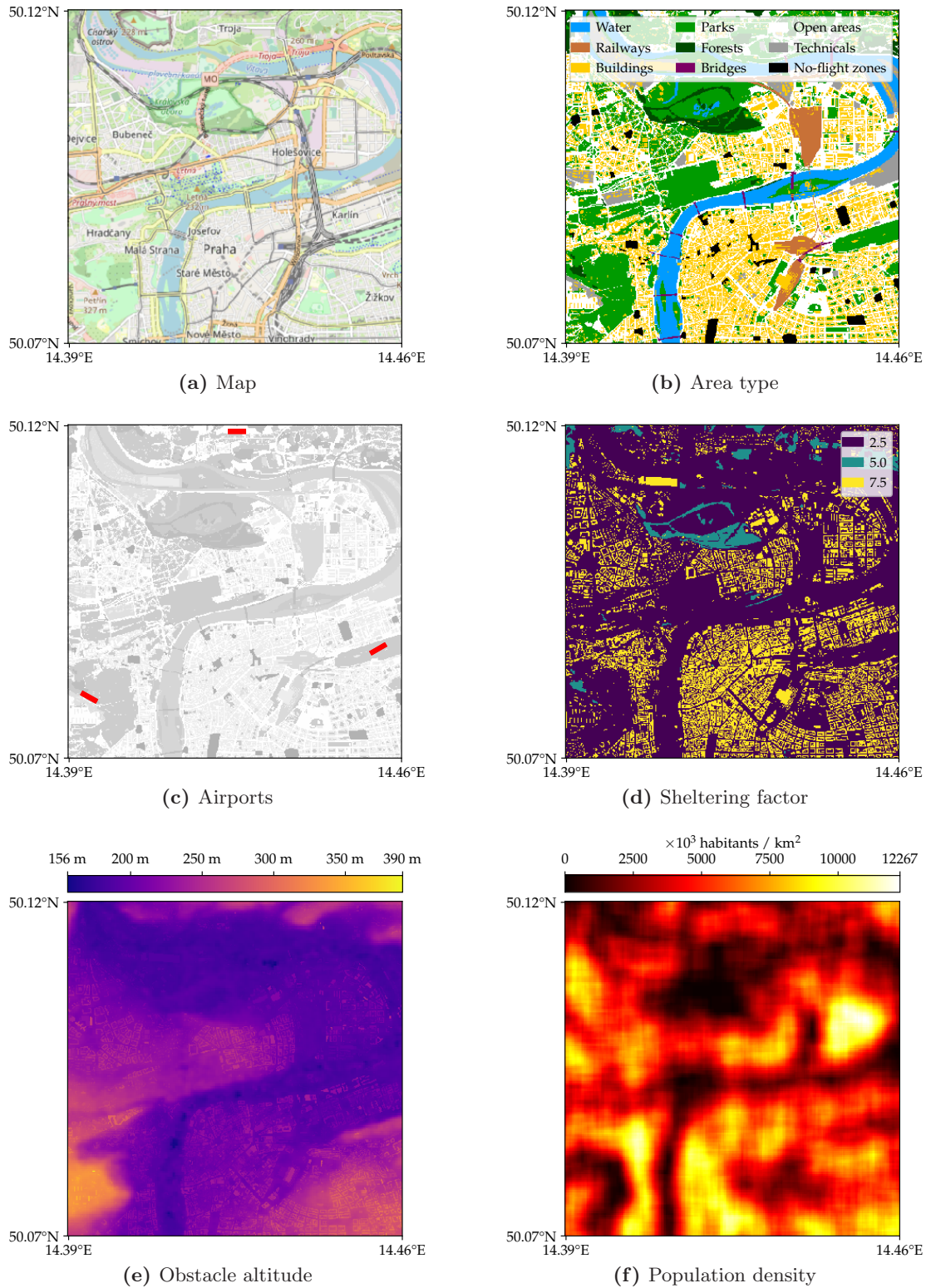


Figure 7.1: Map layers of the created urban scenario based on the Prague city center. The map data are obtained from (OpenStreetMap, 2021), the terrain altitude data are taken from (NASA, 2013), and a real population density from (Facebook, 2016). Three fictional airports are placed around the city to simulate a realistic urban scenario with possible landing sites for a safe emergency landing.

Furthermore, a failure model is also needed. The accident rate and the probability of in-flight loss of thrust are not available for the selected Cessna 172 aircraft (to the best of the authors' knowledge). On the other hand, we may assume that the rates are similar for all general aviation aircraft. Geske (2018) reports on general aviation accidents in the United States in 2015 and reveals the accident rate of 4.89 accidents per 10^5 flight hours. However, only 16% of those have been caused by mechanical issues. The total failure is considered in the herein proposed risk-aware planning. Therefore, omitting reported pilots' mistakes and other unspecified causes leads to the failure rate $p_{\text{fail}} = 10^{-5} \text{ h}^{-1}$.

Geske (2018) reports only accidents, which is an event during which a person receives a fatal or serious injury or any aircraft receives substantial damage as a result of an aircraft operations, according to National Transportation Safety Board¹ (U.S. Code, 1988). In-flight failures followed by a successful emergency landing are not included in the report, and so the in-flight loss of thrust failure rates cannot be retrieved from that report. On the other hand, (ATSB, 2016) of the Australian Transport Safety Bureau² elaborates exactly on the engine failure rates. Based on the reported results, an engine failure rate $p_{\text{fail}}^{\text{LoT}} = 1.3 \cdot 10^{-4} \text{ h}^{-1}$ is used in the presented empirical evaluation.

According to the performance evaluation described in Chapter 6, the parameters of the proposed method are selected as follows. The safe altitude roadmap is expanded for 10 min, which leads to a safe altitude map with $5 \cdot 10^3$ nodes and the mean distance between nodes of 30 m, which is considered sufficiently dense. During the planning phase, each maneuver is sampled with $d_{\text{step}} = 10$ m to check its admissibility. The maximum growth step $\Delta_{\text{step}} = 450$ m is allowed, and a parent for the new sample is found from its $k = 20$ nearest neighbors. Besides, we consider the second settings with $k = 110$, which guarantees the asymptotic optimality of the proposed method. Once the planning roadmap reaches the initial configuration within $\Delta_{\text{tol}} = 450$ m, the planning process is terminated, and the final trajectory is extracted.

7.3 Reference Methods

Solutions found by the proposed method have been compared with two other approaches to elaborate on its performance. A common trajectory planning is to find the shortest trajectory. Therefore, the first baseline reference method is shortest trajectory planning with online emergency situation handling, i.e., a shortest trajectory without emergency landing guarantee is planned, and the emergency landing is solved when loss of thrust occurs. The second method is based on risk-aware trajectory planning (Primatesta et al., 2020b), which, however, needs to be generalized for various flight levels.

7.3.1 Shortest Trajectory Planning Reference Method

The regular RRT* algorithm (Karaman and Frazzoli, 2011) without assuming the risk induced by possible in-flight malfunction is employed to determine the shortest trajectory. If a total malfunction happens during the flight along the planned trajectory, the aircraft falls along a ballistic curve and crashes into the ground. The fall and impact location are given solely by the fall parameters, and a pilot cannot influence them. Therefore, the risk induced by

¹National Transportation Safety Board (NTSB) is the U.S. authority in charge of aircraft accident investigations.

²Australian Transport Safety Bureau (ATSB) is Australia's national transport safety investigator.

the total malfunction for a certain trajectory is evaluated according to (3.5). The risk of the shortest trajectory induced by possible total malfunction is given by (3.3).

However, an emergency landing can be performed in the case of the total loss of thrust. Since the shortest trajectory does not guarantee a safe emergency landing in the case of loss of thrust, a possible landing site and an emergency landing trajectory needs to be determined. The landing site selection and gliding trajectory planning cannot be made instantly because a human pilot would need some time to assess the situation and execute the emergency landing. Also, an autopilot would need some time to select the best landing site and plan the emergency landing trajectory. Hence, we assume a straight flight is maintained for 15 s in the case of the total loss of thrust to simulate the needed decision time. After that, a direct gliding trajectory towards the closest landing site is used as the emergency landing trajectory. If the aircraft can reach the landing site, the induced risk is assumed to be zero. However, suppose the aircraft altitude is not sufficient, and the aircraft crashes during the emergency landing. In that case, the risk of a crash is evaluated according to (3.5), and the risk of the shortest trajectory induced by the possible loss of thrust can be determined by (3.3).

7.3.2 Risk-Aware Trajectory Planning Reference Method

The second reference method is based on the risk-aware trajectory planning proposed by Primatesta et al. (2020b). The method assumes a fixed-flight altitude, and therefore, we generalize it to various flight levels. Moreover, the original method asserts that the impact location cannot be influenced if a failure happens. That assertion complies with our total in-flight malfunction, and the method can find a trajectory minimizing the risk induced by possible total in-flight malfunction.

However, a possibility of an emergency landing in the case of the total loss of thrust is not assumed by Primatesta et al. (2020b). Hence, the risk induced by a possible loss of thrust cannot be utilized in the planning as originally proposed. Therefore, the risk induced by the total loss of thrust along the found trajectory is evaluated similarly as in the reference method based on the shortest trajectory described in Section 7.3.1. A straight flight for 15 s is maintained to mitigate the time needed to select the landing site and determine the emergency landing trajectory. Afterward, the shortest gliding trajectory towards the closest landing site is executed. If the aircraft crashes, the risk induced by loss of thrust at the malfunction configuration is evaluated according to (3.5), and the loss-of-thrust induced risk of the whole trajectory is found using (3.3) similarly to the shortest trajectory reference method.

7.4 Results

The proposed method has been implemented in Julia ver. 1.5.3 (Bezanson et al., 2017), and it has been executed on a single core of the Intel Xeon Scalable Gold 6146 CPU running at up to 3.20 GHz. Each instance of the urban scenario has been solved ten times, and the results are summarized in Table 7.4. An example of a found solution is depicted in Fig. 7.2.

The risk induced by the loss of thrust \mathcal{R}_{LoT} of trajectories without an emergency landing guarantee may be zero, as can be seen for the first and fourth instances in Table 7.4. Such a situation may happen if the trajectory is at a sufficiently high height. Although the reference method offers the shortest trajectory, its risk may vary greatly, as the risk is not considered in the planning. The least risky trajectory (the second reference method) minimizes the risk during the planning phase. However, it minimizes only the risk \mathcal{R} induced by the total

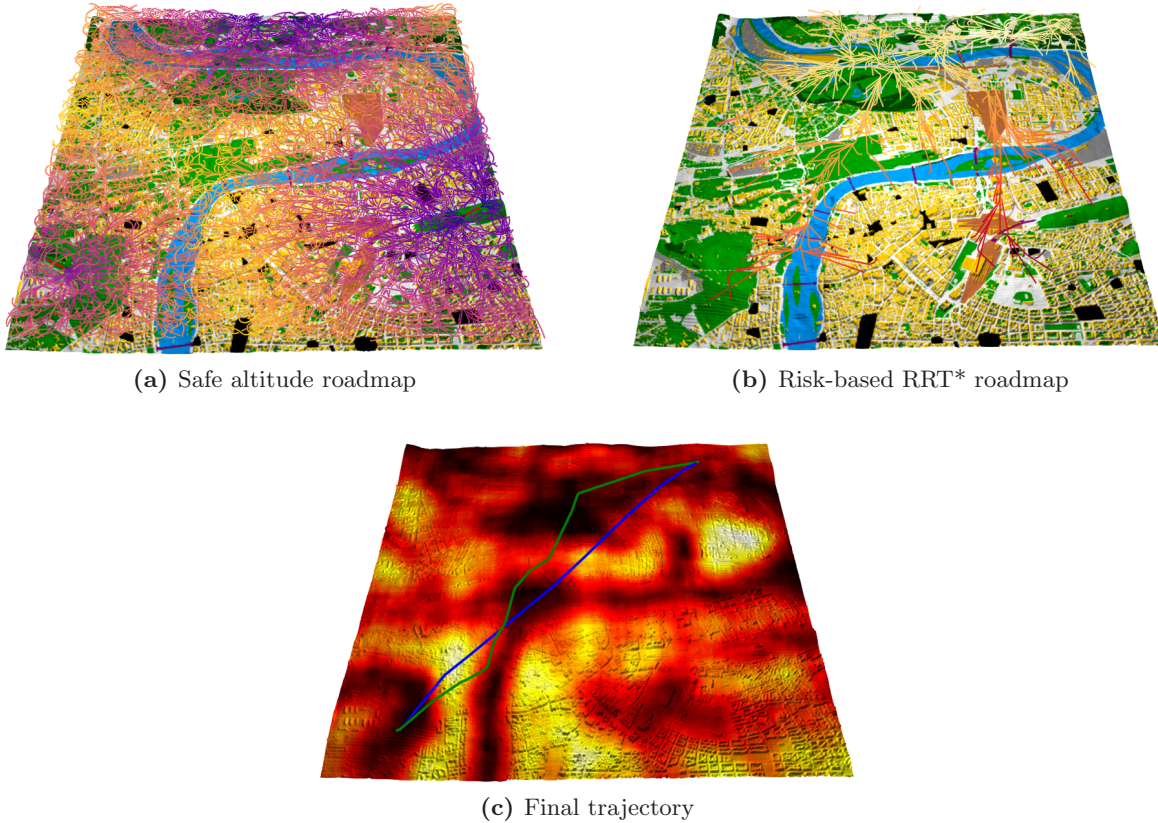


Figure 7.2: An example of the found solution. The pre-computed safe altitude map is shown in (a), with airports depicted as red rectangles. The planning roadmap of the proposed risk-based RRT* method is depicted in (b). The population density is used as a terrain overlay in (c), where the found trajectory is visualized. The found least risky trajectory (in green) is longer than the shortest trajectory (in blue). However, the overall risk of the trajectory is reduced by 95% compared to the shortest trajectory. The proposed algorithm tends to fly over less risky areas, such as rivers and areas with low population density.

malfunction. Therefore, the risk \mathcal{R} of the found trajectory is reduced compared to the shortest trajectory. The method is not capable of estimating the risk \mathcal{R}_{LoT} induced by the total loss of thrust, and thus reducing the risk \mathcal{R} may increase the risk \mathcal{R}_{LoT} as the trajectory deviates to areas with lower risk \mathcal{R} but more severe consequences of the loss of thrust. Since the loss of thrust is more likely to happen than the total malfunction, the overall trajectory risk \mathcal{R}_{tot} may increase compared to the shortest trajectory; see the third planning instance in Table 7.4.

The proposed method guarantees safe emergency landing in the case of loss of thrust. The guarantee may not allow the aircraft to visit areas with the lowest risk induced by the total malfunction as the safe landing would not be possible from those areas. Hence, it restricts the planning space, and the risk \mathcal{R} may slightly increase compared to the least risky trajectory; see the second planning instance in Table 7.4. Nevertheless, the risk \mathcal{R}_{LoT} induced by the possible loss of thrust is always zero due to the guaranteed safe emergency landing. The overall risk is reduced compared to the least risky trajectory approach as the loss of thrust is more likely to happen. Finally, the resulting trajectory may be significantly prolonged compared to the shortest trajectory planned without any risk taken into account, but the total risk is significantly lower. Therefore, the proposed method finds trajectories minimizing the overall

Table 7.4: Results summary showing median values from 10 independent runs. The trajectory length is \mathcal{L} , overall risk \mathcal{R}_{tot} , and needed computational time t_{CPU} . The overall risk \mathcal{R}_{tot} consists of the risk \mathcal{R} induced by the total in-flight malfunction and the risk \mathcal{R}_{LoT} induced by possible in-flight loss of thrust. Note that the risks are shown in the number of casualties.

Shortest path					Least risky path				
\mathcal{L}	\mathcal{R}	\mathcal{R}_{LoT}	\mathcal{R}_{tot}	t_{CPU}	\mathcal{L}	\mathcal{R}	\mathcal{R}_{LoT}	\mathcal{R}_{tot}	t_{CPU}
[km]	$[\times 10^{-5} \text{ cas.}]$	$[\times 10^{-5} \text{ cas.}]$	$[\times 10^{-5} \text{ cas.}]$	[s]	[km]	$[\times 10^{-5} \text{ cas.}]$	$[\times 10^{-5} \text{ cas.}]$	$[\times 10^{-5} \text{ cas.}]$	[s]
2.0	4.8	0.0	4.8	47.8	2.1	4.6	0.0	4.6	359.3
3.1	7.6	8.0	15.5	53.4	4.6	4.7	35.0	39.7	935.9
3.3	6.4	0.0	6.4	56.9	3.8	5.5	53.7	59.2	875.6
3.3	4.7	0.0	4.7	227.3	4.0	3.7	0.0	3.7	802.5
5.3	10.5	163.0	173.5	204.5	5.8	5.8	98.5	104.3	298.7

Proposed path with emergency landing guarantee in the case of loss of thrust									
$k = 20$					$k = 110$				
\mathcal{L}	\mathcal{R}	\mathcal{R}_{LoT}	\mathcal{R}_{tot}	t_{CPU}	\mathcal{L}	\mathcal{R}	\mathcal{R}_{LoT}	\mathcal{R}_{tot}	t_{CPU}
[km]	$[\times 10^{-5} \text{ cas.}]$	$[\times 10^{-5} \text{ cas.}]$	$[\times 10^{-5} \text{ cas.}]$	[s]	[km]	$[\times 10^{-5} \text{ cas.}]$	$[\times 10^{-5} \text{ cas.}]$	$[\times 10^{-5} \text{ cas.}]$	[s]
2.0	4.7	0.0	4.7	220.5	2.0	4.6	0.0	4.6	2372.2
4.4	4.8	0.0	4.8	216.4	4.7	4.6	0.0	4.6	7297.3
3.8	5.7	0.0	5.7	405.7	3.8	5.4	0.0	5.4	3511.7
4.0	3.7	0.0	3.7	257.7	3.9	3.6	0.0	3.6	10199.5
5.9	6.0	0.0	6.0	224.4	5.8	5.8	0.0	5.8	3700.9

risk induced by the total malfunction and loss of thrust. Furthermore, it can be noticed that using the higher value of k provides better results; however, it is at the cost of about two orders of magnitude higher computational requirements.

7.4.1 Discussion

Based on the reported results, it can be concluded that a risk of an arbitrary trajectory may vary a lot. In some cases, the risk induced by loss of thrust is zero, as the safe emergency landing is possible even if it is not accounted for. In those cases, the risk-based trajectory planning adopted from Primatesta et al. (2020b) offers the same solution as the proposed method, but it requires less computational time. If the safe emergency landing is not guaranteed, the found trajectories of both reference methods are burdened with a risk induced by loss of thrust. Since the loss of thrust is significantly more likely to happen than the total failure, \mathcal{R}_{LoT} may be significantly larger than \mathcal{R} . Then, the proposed method finds a trajectory with a guaranteed safe landing option and minimal risk induced by the total malfunction. As the former usually account for most of the overall trajectory risk in both reference methods, the proposed method offers a significantly less risky trajectory.

Therefore, the proposed method provides trajectories with a guaranteed emergency landing in the case of loss of thrust while minimizing the risk to people on the ground induced by possible in-flight total malfunction. Hence, the overall trajectory risk is significantly reduced. In particular, the overall risk has been reduced by up to 95 % in the evaluated cases compared to the reference methods.

*Chapter 7. Evaluation of the Proposed Risk-aware Trajectory Planning with Safe
Emergency Landing Guarantee*

Conclusion

In this thesis, a risk-aware trajectory planning problem in an urban environment is studied. An in-flight failure poses a risk to people on the ground, especially when flying in urban environments with high population density. Therefore, the goal is to minimize the risk to people on the ground induced by possible in-flight failure. An aircraft might perform an emergency landing in the case of a partial loss of control, such as loss of thrust, resulting in a crash if a landing site is not within a gliding range of the aircraft. Our proposed method combines risk-aware trajectory planning with the safe emergency landing guarantee throughout the whole trajectory. The risk-aware trajectory planning method allows planning trajectories to minimize the risk in the case of a crash, while the safe emergency landing guarantee prevents the crash in the case of loss of thrust. The proposed method has been empirically evaluated on a realistic urban scenario. It has been compared to the shortest trajectory and existing risk-aware trajectory planning extended for various flight altitudes.

The trajectories provided by the proposed method are less risky than the shortest ones as detours over less risky areas are preferred. Furthermore, the safe emergency landing guarantee eliminates the risk induced by loss of thrust, and the overall risk is significantly reduced. Hence, a lower risk is achieved compared to shortest and risk-aware only trajectories, which may lead to a crash even in the loss of thrust. Based on the reported results, the proposed method provides significantly less risky trajectories than the current state-of-the-art approaches as the risk reduction of up to 95% has been achieved. The proposed method seems to be a suitable choice for trajectory planning in urban air mobility scenarios.

In our future work, we would like to verify our results on a real general aviation aircraft. Besides, we aim to extend the proposed solution further to account for dynamic obstacles, such as other aircraft. Furthermore, we would like to generalize the proposed method into a general planning-in-planning framework to plan trajectories while some safety options are guaranteed. For example, imagine a fleet of UAVs that are tasked to deliver various packages. The UAVs might be required at any time to land at any of the given depots due to unforeseen reasons, such as a change in the weather forecast. Since the forced landing is a stand-alone trajectory planning problem, the generalized framework would allow planning the delivery tasks such that the unforeseen forced landing is guaranteed within a given time. On top of that, the planning of forced landing would have to consider the sequence of landing in the case of a fleet forced landing as the landing site can be used by only one UAV at a time. That is an additional challenge that might be addressed to support practical deployments.

Bibliography

- 49 CFR Part 830 (1988). Notification and reporting of aircraft accidents or incidents and overdue aircraft, and preservation of aircraft wreckage, mail, cargo, and records. <https://www.law.cornell.edu/cfr/text/49/part-830>. Accessed on: 24 May 2021.
- ATAG, Air Transport Action Groupe (2019). Aviation benefits beyond borders.
- Atkins, E. (2010). Emergency landing automation aids: an evaluation inspired by us airways flight 1549. In *AIAA Infotech@ Aerospace*, page 3381.
- Australian Transport Safety Bureau (2016). Engine failures and malfunctions in light aeroplanes 2009 - 2014. *Investigation number AR-2013-107, 9 March 2016*, pages 1–38.
- Bezanson, J., Edelman, A., Karpinski, S., and Shah, V. B. (2017). Julia: A fresh approach to numerical computing. *SIAM review*, 59(1):65–98.
- CASA (2007). *Visual Flight Rules Guide*. Canberra: Civil Aviation Safety Authority Australia (CASA).
- Chitsaz, H. and LaValle, S. M. (2007). Time-optimal paths for a dubins airplane. In *IEEE CDC*, pages 2379–2384.
- Civil Aviation Authority (2019). *Letecký předpis L2: Pravidla létání*. Ministry of Transportation of the Czech Republic.
- Dalamagkidis, K., Valavanis, K., and Piegl, L. (2009). On integrating unmanned aircraft systems into the national airspace system, international series on intelligent systems, control, and automation: Science and engineering. *Science and Engineering*, 36.
- Desaraju, V. R., Michael, N., Humenberger, M., Brockers, R., Weiss, S., Nash, J., and Matthies, L. (2015). Vision-based landing site evaluation and informed optimal trajectory generation toward autonomous rooftop landing. *Autonomous Robots*, 39(3):445–463.
- Dijkstra, E. W. (1959). A note on two problems in connexion with graphs. *Numerische mathematik*, 1(1):269–271.
- Dubins, L. E. (1957). On curves of minimal length with a constraint on average curvature, and with prescribed initial and terminal positions and tangents. *American Journal of mathematics*, 79(3):497–516.
- Eng, P. (2011). *Path planning, guidance and control for a UAV forced landing*. PhD thesis, Queensland University of Technology.

Bibliography

- Facebook Connectivity Lab and Center for International Earth Science Information Network - CIESIN - Columbia University (2016). High Resolution Settlement Layer (HRSL). Source imagery for HRSL © 2016 DigitalGlobe.
- Faigl, J. and Váňa, P. (2018). Surveillance planning with bézier curves. *IEEE Robotics and Automation Letters*, 3(2):750–757.
- Geske, R. C. (2018). *27th Joseph T. Nall Report*. Richard G. McSpadden, JR.
- Hart, P., Nilsson, N., and Raphael, B. (1968). A formal basis for the heuristic determination of minimum cost paths. *IEEE Transactions on Systems Science and Cybernetics*, 4(2):100–107.
- Hu, X., Pang, B., Dai, F., and Low, K. H. (2020). Risk assessment model for uav cost-effective path planning in urban environments. *IEEE Access*, 8:150162–150173.
- Humbard, J. J. and Putman, J. (2007). Flight management system and method for providing navigational reference to emergency landing locations. US Patent 7,167,782.
- IATA (2021). Fact sheet: Safety. <https://www.iata.org/en/iata-repository/pressroom/fact-sheets/fact-sheet---safety/>. Accessed on: 1 April 2021.
- ICAO (2019). Aviation benefits report 2019. Industry High Level Group.
- Kan, E.-M. et al. (2011). Contour based path planning with b-spline trajectory generation for unmanned aerial vehicles (uavs) over hostile terrain. *Journal of Intelligent Learning Systems and Applications*, 3(03):122.
- Karaman, S. and Frazzoli, E. (2011). Sampling-based algorithms for optimal motion planning. *International Journal of Robotics Research*, 30(7):846–894.
- Kavraki, L. E., Svestka, P., Latombe, J.-C., and Overmars, M. H. (1996). Probabilistic roadmaps for path planning in high-dimensional configuration spaces. *IEEE transactions on Robotics and Automation*, 12(4):566–580.
- Koenig, S. and Likhachev, M. (2005). Fast replanning for navigation in unknown terrain. *IEEE Transactions on Robotics*, 21(3):354–363.
- Kuffner, J. J. and LaValle, S. M. (2000). Rrt-connect: An efficient approach to single-query path planning. In *ICRA*, volume 2, pages 995–1001.
- la Cour-Harbo, A. (2020). Ground impact probability distribution for small unmanned aircraft in ballistic descent. In *International Conference on Unmanned Aircraft Systems (ICUAS)*, pages 1442–1451.
- LaValle, S. M. (1998). Rapidly-exploring random trees : a new tool for path planning. *The annual research report*.
- McLain, T., Beard, R. W., and Owen, M. (2014). Implementing dubins airplane paths on fixed-wing uavs. In Valavanis, K. P. and Vachtsevanos, G. J., editors, *Handbook of Unmanned Aerial Vehicles*, pages 1677–1701. Springer Netherlands.
- Mejias, L. and Fitzgerald, D. (2013). A multi-layered approach for site detection in uas emergency landing scenarios using geometry-based image segmentation. In *Unmanned Aircraft Systems, International Conference on*, pages 366–372. IEEE.
- Moore, M. (2003). 21st century personal air vehicle research. In *AIAA International Air and Space Symposium and Exposition: The Next 100 Years*, page 2646.
- NASA, Jet Propulsion Laboratory (2013). Nasa shuttle radar topography mission global 1 arc second. <https://opentopography.org/>. Accessed on: 10 February 2021.
- Neto, A. A., Macharet, D. G., and Campos, M. F. (2015). 3d path planning with continuous bounded curvature and pitch angle profiles using 7th order curves. In *IEEE/RSJ International Conference on Intelligent Robots and Systems (IROS)*, pages 4923–4928.

- Noreen, I., Khan, A., and Habib, Z. (2016). Optimal path planning using rrt* based approaches: A survey and future directions. *International Journal of Advanced Computer Science and Applications*, 7.
- OpenStreetMap contributors (2021). Planet dump retrieved from <https://planet.osm.org>. Accessed on: 24 May 2021.
- Otte, M. and Frazzoli, E. (2016). Rrtx: Asymptotically optimal single-query sampling-based motion planning with quick replanning. *International Journal of Robotics Research*, 35(7):797–822.
- Patrikar, J., Dugar, V., Arcot, V., and Scherer, S. (2020). Real-time motion planning of curvature continuous trajectories for urban uav operations in wind. In *2020 International Conference on Unmanned Aircraft Systems (ICUAS)*, pages 854–861. IEEE.
- Penrose, M. (2003). *Random geometric graphs*. Oxford university press.
- Primatesta, S., Guglieri, G., and Rizzo, A. (2019). A risk-aware path planning strategy for uavs in urban environments. *Journal of Intelligent & Robotic Systems*, 95(2):629–643.
- Primatesta, S., Rizzo, A., and la Cour-Harbo, A. (2020a). Ground risk map for unmanned aircraft in urban environments. *Journal of Intelligent & Robotic Systems*, 97(3):489–509.
- Primatesta, S., Scanavino, M., Guglieri, G., and Rizzo, A. (2020b). A risk-based path planning strategy to compute optimum risk path for unmanned aircraft systems over populated areas. In *International Conference on Unmanned Aircraft Systems (ICUAS)*, pages 641–650.
- Rackauckas, C. and Nie, Q. (2017). Differentialequations.jl—a performant and feature-rich ecosystem for solving differential equations in julia. *Journal of Open Research Software*, 5(1).
- Savage, I. (2013). Comparing the fatality risks in united states transportation across modes and over time. *Research in transportation economics*, 43(1):9–22.
- Sláma, J. (2018). Emergency landing guidance for an aerial vehicle with a motor malfunction. *Bachelor’s Thesis, Czech Technical University in Prague, Czech Republic*.
- Standard, RCC (2007). 321-07, common risk criteria for national test ranges. range safety group risk committee, range commanders council. *US Army White Sands Missile Range, New Mexico*.
- Truong, D. and Choi, W. (2020). Using machine learning algorithms to predict the risk of small unmanned aircraft system violations in the national airspace system. *Journal of Air Transport Management*, 86:101822.
- Váňa, P., Neto, A. A., Faigl, J., and Macharet, D. G. (2020a). Minimal 3d dubins path with bounded curvature and pitch angle. In *IEEE International Conference on Robotics and Automation (ICRA)*, pages 8497–8503.
- Váňa, P., Sláma, J., and Faigl, J. (2020b). Surveillance planning with safe emergency landing guarantee for fixed-wing aircraft. *Robotics and Autonomous Systems*, 133:103644.
- Váňa, P., Sláma, J., Faigl, J., and Pačes, P. (2018). Any-time trajectory planning for safe emergency landing. In *IEEE/RSJ International Conference on Intelligent Robots and Systems (IROS)*, pages 5691–5696.
- Wang, Y., Wang, S., Tan, M., Zhou, C., and Wei, Q. (2014). Real-time dynamic dubins-helix method for 3-d trajectory smoothing. *IEEE Transactions on Control Systems Technology*, 23(2):730–736.
- Wright, O. et al. (1977). *How we made the first flight*. Department of Transportation, Federal Aviation Administration, Office of General Aviation Affairs.

